Data Analytics MSc Dissertation MTHM038, 2022/23

Estimating source properties of gravitational waves from collisions of black holes

Dhruv Vudayagiri, ID 220375472

Supervisor: Prof. Hong Qi

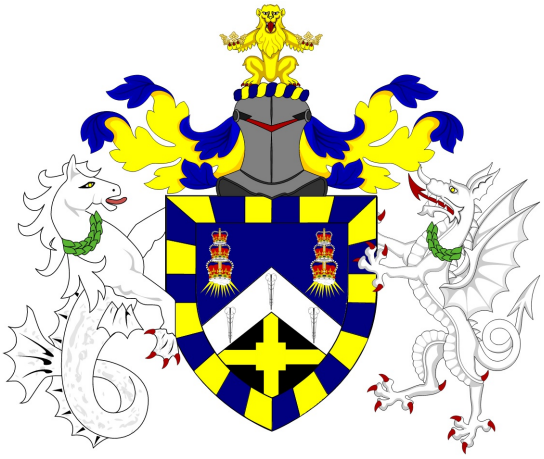

A thesis presented for the degree of

Master of Science in *Data Analytics*

School of Mathematical Sciences

Queen Mary University of London

Declaration of original work

This declaration is made on September 4, 2023.

Student's Declaration: I Dhruv Vudayagiri hereby declare that the work in this thesis is my original work. I have not copied from any other students' work, work of mine submitted elsewhere, or from any other sources except where due reference or acknowledgement is made explicitly in the text, nor has any part been written for me by another person.

Referenced text has been flagged by:

1. Using italic fonts, **and**
2. using quotation marks "...", **and**
3. explicitly mentioning the source in the text.

Acknowledgements

I would like to express my sincere gratitude to Dr. Hong Qi, my esteemed professor at Queen Mary University of London, for her great advice, mentoring, and steadfast support during the whole of my thesis endeavour. The extensive knowledge and experience of Dr. Qi have made a substantial contribution to this scientific endeavour, serving as a source of inspiration for me to pursue greatness.

I would like to acknowledge the Laser Interferometer Gravitational-Wave Observatory (LIGO) for its provision of vital data and background information, which served as the fundamental basis for this thesis. The use of LIGO's resources has facilitated the expansion of my scientific endeavours, enabling me to delve into the realm of Gravitational Waves and Binary Black Holes.

My heartfelt thanks to my colleagues and peers for their support, which have greatly enhanced the academic nature of our attempt.

I would like to extend my profound gratitude to my family and friends for their support, understanding, and encouragement during the arduous stages of this scientific endeavour.

Each individual involved made an essential contribution to the successful completion of my thesis, and I express sincere appreciation for their efforts.

Abstract

The detection of gravitational waves since 2015 has transformed astrophysics, providing a unique perspective on the universe. The project is centred on estimating the source properties of gravitational waves resulting from black hole collisions, an increasingly significant research area. Previous studies confirmed gravitational waves' existence, mainly those generated by compact binary systems like black hole mergers. The methodology relies on statistical techniques such as Bayesian inference, Markov Chain Monte Carlo, and the Dynesty sampler to estimate source parameters for gravitational wave signals. The analysis section presents results, including GW150914 analysis with different parameter settings, similar gravitational wave injections in various observational runs (O1, O2, and O3), and simulations of future detector networks. These results encompass comprehensive GW150914 analyses, insights into injected gravitational wave properties in different observational runs, and statistical assessments of mass ratios and spin uncertainties. Additionally, the project introduces the concept of a future detector network (HLV) and explores its potential impact on gravitational wave analysis. This study advances understanding of gravitational waves from black hole collisions. Future research can expand detector networks, improve estimation techniques, and investigate additional gravitational wave sources, deepening cosmic insights.

Contents

Chapter 1

Introduction

1.1 Overview

The identification of gravitational waves in the year 2015 was a significant milestone in the field of astronomy, presenting new insights into the nature of the cosmos. This dissertation undertakes an investigation into the complex characteristics of cosmic occurrences, specifically concentrating on the estimation of attributes of gravitational waves generated by the intense collisions of black holes.

The introductory section will provide a comprehensive summary of the accomplishments of the project. The investigation has yielded novel discoveries that provide light on gravitational waves, namely those generated by the merging of black holes. These findings has the potential to enhance our comprehension of these mysterious phenomena.

To achieve the aforementioned objectives, the research used robust statistical techniques like Bayesian inference, Markov Chain Monte Carlo, and the Dynesty sampler. These methodologies have facilitated the determination of the parameters associated with the transmission of gravitational waves, yielding valuable findings that have broader ramifications extending beyond the immediate scope.

The dissertation will use actual situations to illustrate the pragmatic importance of the research. The subsequent examples will effectively demonstrate the pragmatic ramifications of these findings and their pertinence to the comprehension of the cosmos.

As the ongoing research advances, the study endeavours to look into the interconnections that have been shown between different aspects of astrophysics and detector technology. The aforementioned connections indicate promising prospects for the incorporation of forthcoming detector networks, hence augmenting the potential for gravitational wave analysis.

The study further derives advantages from rigorous computational analyses using sophisticated methodologies such as Bayesian inference and Markov Chain Monte Carlo. The use of computing methods in these scientific activities guarantees a high level of accuracy and thoroughness in the investigations, therefore yielding significant insights into the complex characteristics of gravitational waves produced by the collisions of black holes.

The introductory section lays the groundwork for the subsequent chapters, encouraging readers to engage in an exploratory journey as the enigmas surrounding gravitational waves are unravelled, so enhancing our understanding of the cosmos.

1.2 General relativity

In "general relativity", a combination of geometric and physical laws provides a set of Einstein field equations for the gravitational field as well as geodesic equations for light transmission and background particle motion[1]. A precise formulation for gravitational waves was first put forth by Einstein in 1916 and 1918[2]. He compared the theory of relativity with Newton's theory and expressed the simplest form of Newton's theory. Gravitational waves are the last prediction of the theory of general relativity, and its future examination will be addressed in the next section.

1.3 Gravitational waves

When cataclysmic events like collisions of binary black holes[3], neutron stars[4], or supernovae[5] (which occur when the stars reach their lifetime and explode) happen, the space will be stretched and squeezed as ripples travel in all directions known as gravitational waves (GWs), and when they pass through the universe at the speed of light, there is a change in the curvature of the object. Hence, it can be learned by calculating the difference in the length of objects, known as strain.

As per Einstein's special theory of relativity, apart from three-dimensional space, it also includes time, which is part of it and shares it with four-dimensional space. But as per general relativity, he explained that in addition to interconnecting them further, they are bent due to the presence of masses or energy, resulting in a curved space. So, when events related to cataclysmic physics occur, these masses or energies will change the curvature of space around them[6].

According to this theory, Einstein predicted GWs, but two scientists proved it in 1974 with the aid of the Arecibo radio observatory located in Puerto Rico and revealed the existence of binary pulsars[7] (a pulsar rotates around either another star or a pulsar) existing about 21 thousand light years away from the earth. Pulsars are rotating neutrons that emit radiation. With these findings, many studies were conducted around them and found similar effects, proving the existence of GWs.

The discovery of GWs marks a major achievement in the ongoing century-old advancement of this scientific theory. Back on September 14, 2015, the collision of two black holes led to the detection of GWs, often called "gravitational radiation," using interferometer sensors. A black hole is an area in space-time where the gravitational pull is so powerful that even light cannot escape and reach infinity[8], which leads scientists to observe the universe and cataclysmic events from a different perspective.

In the field of physics, GWs concealed wide-ranging information related

to strong-field gravitation, like the origin and type of objects involved in the generation. Using this information, we can approximate the mass and location of the event, as the wave frequency determines the mass of the object, whereas the strength of the GWs informs the location. Apart from that, we can all determine all the other specifications related to it, such as luminosity distance[9], orbital inclination angle[10], etc. Generally, the oscillation period of events related to astrophysics ranges from 1 millisecond to hours[11].

Prior to the use of gravitational waves (GWs) in the field of astrophysics for the purpose of comprehending the workings of the universe, the transmission of information was mostly reliant on light signals. So, GWs stood out as an edge towards the advantage of understanding the incidents before the mergers and using that information to correlate the merger information with the real-time data that was detected.

1.3.1 Gravitational wave types

The gravitational waves (GWs) were classified into four distinct categories by astrophysicists. Each entity has distinct attributes that set it apart from others and contribute to its significance in data analysis for signal study.

1.3.2 Compact binary inspiral gravitational waves

All observed waves will be categorised inside this specific category. Within this categorization, there are further subcategories, including Binary Neutron Star (BNS), Binary Black Hole (BBH), and Neutron Star-Black Hole binary (NSBH). Every individual thing has its own pattern; yet, the mechanism via which waves are produced by massive and compact phenomena like BBHs and neutron stars stays constant. Each individual item has its own unique pattern; nevertheless, the generation of waves by massive and dense entities like as BBHs and BNS follows a similar mechanism, often known as the Inspiral phenomena. The occurrence of GWs emission is seen when two

objects engage in rotating motion with respect to one other. Interferometers are deliberately designed to possess a level of sensitivity, hence facilitating their ability to detect waves within a certain range. Interferometers have the potential to detect the emission of GWs during the pre-merger phase of these events. The emissions in question have a limited duration, lasting just for a fraction of a second, and display distinct features.

1.3.3 Other types

Continuous gravitational waves When a BNS, undergoes rotational motion, it is postulated that the presence of irregularities or deformations may be seen inside its structure. During the spin, it produces GWs that propagate in a radial manner. Moreover, in the event of a continuous rotational motion, GWs would have same frequencies and amplitudes. These phenomena were often referred to be continuous GWs. However, the detection of these phenomena not yet been achieved, although researchers have conducted simulations in order to get insight into their potential characteristics.

Stochastic gravitational waves Stochastic means random wave data that can be measured mathematically but cannot be observed. Since these are very small GWs that pass through everything in the universe, including earth, the existing detectors were not that sensitive to detect them. But scientists believe that these contain a small portion of information that may describe the big bang mixed with noise.

Burst gravitational waves Assuming a limited knowledge of physics, it becomes challenging to understand these phenomena that arise from unidentified sources. The prediction of GWs that traverse the Earth is challenging due to their distinct features, compared to other forms of GWs. The identification of these patterns proved challenging due to their lack of modelling and their complexity, perhaps surpassing human cognitive capacities. The detection of burst GWs is a challenging task, although it offers a unique opportunity to get novel insights into the realm of space.

Chapter 2

Gravitational wave detectors

2.1 Principles of interferometers

Black holes are the densest objects created from the deaths of massive stars. As these orbited each other, characteristic patterns of ripples were produced. These ripples in spacetime are the GWs moving away, similar to the speed of light. While they were travelling, the stretching and squeezing cause a loss of energy. So, while the energy gradually reduces, they spiral and orbit each other faster and quicker, until they finally merge and release a big burst of GWs.

As these GWs pass through every object, they make them stretch in one direction, squeeze in another direction, and oscillate. But the effect is quite small. So, to detect them, we use detectors placed in different places around the world. These detectors look like giant L-shaped structures known as Michelson interferometers [8].

One of the techniques used for the detection of GWs is described below. In this setup, a laser beam is directed towards a beam splitter, splits the beam into two. The two beams propagate along the arms of the detector, undergo reflection upon encountering the mirrors or test masses positioned at the ends of the arms, and subsequently reunite at the beam splitter, resulting

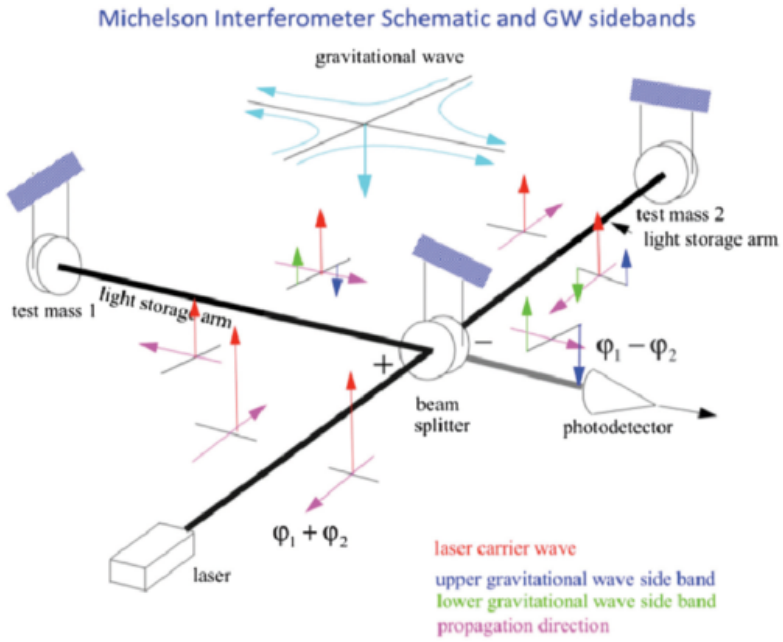

Figure 2.1: Interferometer setup for gravitational wave detection. Source: [12].

in the generation of an output.

When a gravitational wave passes through this, one arm gets stretched while the other is squeezed. The experiment is set up so that when the laser light is recombined, the two waves are equal and opposite to each other, resulting in destructive interference. But when a gravitational wave passes the arms, they are stretched and squeezed. So, the two waves vary in and out of each other, resulting in a split on the screen when the waves are constructively interfering. There are numerous technical difficulties in detecting GWs due to their small effect, including seismic oscillations, scattering, thermal variations, quantum noise, and laser variation.

To improve sensitivity, the laser beam oscillates between reflections within the arms. Sensitivity rises as noise reduces. The detectors are sensitive enough to detect billions and trillions of microns, or 1/1000th the width of a proton. Comparing the measured signal to the predicted signals may reveal

the gravitational wave source due to the system's sensitivity. Black hole masses and distances may be calculated using theoretical models.

In the subsequent sections, a comprehensive exploration of the detectors strategically positioned across the Earth will be undertaken, offering essential insights into the critical aspects of the detectors' design, function, and significance in the field of gravitational wave research.

2.2 LIGO

The Laser Interferometer Gravitational-Wave Observatory (LIGO) represents a transformative effort in astrophysics, directly detecting GWs as predicted by Einstein's general theory of relativity. Utilising advanced detectors and interferometers, LIGO precisely measures GWs by monitoring the displacement of mirrors caused by their passage. Operational oversight is jointly managed by the Massachusetts Institute of Technology (MIT) and the California Institute of Technology (Caltech), with funding from the American National Science Foundation.

In astrophysics, LIGO is pivotal in detecting GWs originating from diverse sources, including binary black holes, binary neutron stars, core collapses leading to type II supernovae, rapidly rotating non-axisymmetric NSs, and even early universe processes generating a stochastic background of GWs [13]. LIGO is primarily designed for GWs with a duration exceeding 100 milliseconds.

LIGO has evolved significantly:

Initial LIGO (iLIGO): Launched in 1999 and operational from 2002 to 2010, iLIGO had a detection range of approximately 15 megaparsecs(Mpc), equivalent to about 46 million light-years. While no GWs were detected during this period, iLIGO laid the foundation for subsequent phases.

Advanced LIGO (aLIGO): Introduced in 2015, aLIGO conducted three observation runs (O1, O2, and O3), significantly extending the BNS merger

detection range to approximately 135 Mpc or 440 million light-years. Compared to iLIGO, aLIGO offers three times the range, ten times the sensitivity, and covers nearly 1000 times the volume in space. In the inaugural phase of O1, both LIGO interferometers in Livingston, LA, and Hanford, WA, jointly detected GWs from the collision of two BBHs located about 1.3 billion light-years away.

2.3 Virgo

Gravitational wave astronomy relies on the Virgo Interferometer at Cascina, Italy, and other observatories like LIGO. In 1993, the Virgo Collaboration was formed to build a cutting-edge gravitational wave detector. The detector has two 3-kilometer arms at right angles. High-power lasers are divided and recombined along these arms to monitor microscopic distance changes between test masses using laser interferometry. Virgo is sensitive enough to detect binary black hole and neutron star mergers because to noise reduction and environmental isolation. Astrophysics and the cosmos have been considerably improved by Virgo's results, an important turning point in GW research.

2.4 KAGRA

Gravitational wave astronomy relies on the Kamioka Gravitational Wave Detector (KAGRA) at Japan's Kamioka Mozumi mine. It uses laser interferometry with two 3-kilometer-long arms in an L-shape to detect small distance changes produced by gravitational waves (GWs), like LIGO and Virgo. Cryogenic technology cools KAGRA's mirrors and other components to very low temperatures. This method decreases thermal noise, improving the detector's GW sensitivity. The worldwide network of gravitational wave detectors and KAGRA work together to detect and analyse gravita-

tional wave occurrences. Its scientific goals include observing and exploring gravitational wave sources like BBH-neutron star mergers, which advances astrophysics and basic physics. KAGRA has helped us solve the universe's secrets via gravitational wave studies since its founding.

2.5 Observations of LIGO, Virgo & KAGRA

- **O1**: Two LIGO detectors participated in this four-month period from September 2015 through January 2016. During its operation, interferometers found three black hole collision-related GWs. After LIGO was improved, further enhancements were performed before O2.
- **O2**: Started November 2016 and finished August 2017. This run, performed by the European Gravitational Observatory from Cascina, Italy, included Virgo and LIGO interferometers. The discovery of the first neutron star collision and eight others during this mission was groundbreaking.
- **O3**: During this run, the interferometers related to Virgo and LIGO were part of this. Which ran from April 2019 to March 2020. At that time, upgrades were made, which resulted in the detection of about 79 events.

Table 2.1: Timeline of Observation Runs and Detectors

OBSERVATION	TIMELINE	DETECTORS
O1	September 2015 – January 2016	LIGO
O2	November 2016 – July 2017	LIGO
O2	August 2017	LIGO and Virgo
O3	April 2019 – March 2020	LIGO and Virgo
O3	April 2020	GEO and KAGRA

The 25-month monitoring period saw 90 merger collision incidents. Later, it received additional improvements, most of which prepared it for the 2023 O4 run. After this improvement, it will be able to detect objects 10 times deeper than the iLIGO in the universe of around 190 Mpc.

2.6 Detector sensitivity

In the field of gravitational wave research, a profound comprehension of detector sensitivity is indispensable. Detector sensitivity plays a pivotal role in our ability to detect and analyse gravitational wave signals effectively. One key concept that underpins this understanding is Power Spectral Density.
Power Spectral Density (PSD): The concept being discussed is a basic principle that pertains to the distribution of power inside a transmission across various frequencies. This study primarily elucidates the magnitude of a signal across several frequencies. Put simply, it denotes the magnitude of power present in a signal across different frequencies. The comprehension of noise and detector sensitivity is of utmost significance in the context of gravitational data analysis.

The graph shown depicts the Power Spectral Density (PSD) of noise seen in two gravitational wave detectors, namely the LIGO and Virgo detectors. The Power Spectral Density (PSD) acts as a visual representation that offers insights into the allocation of signal power across different frequencies. The study of gravitational waves has considerable significance within the realm of academic inquiry.

The graph illustrates the fluctuations in noise levels shown by the detectors throughout a wide range of frequencies, ranging from 10 Hz to 2000 Hz. The comprehension of the detectors' sensitivity and behavioural features may be enhanced by this information. This has great importance as it allows scientists to differentiate gravitational wave signals from the ambient background noise.

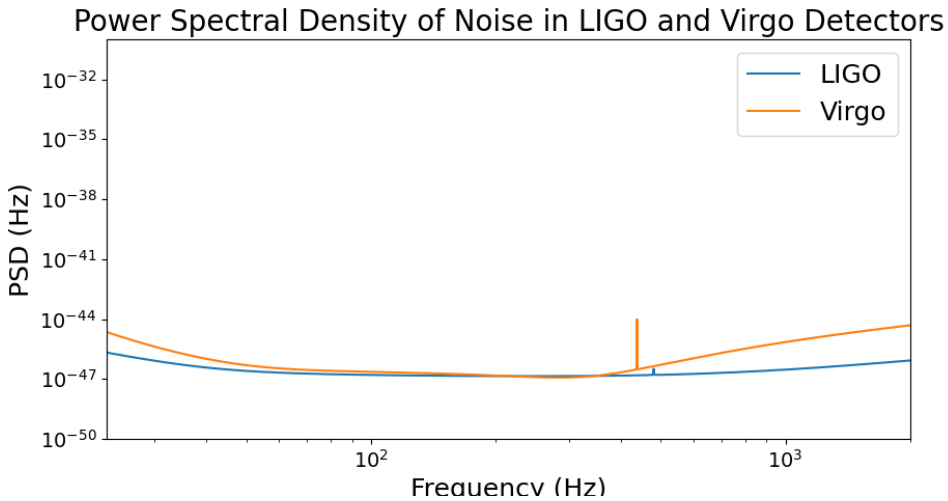

Figure 2.2: PSD for LIGO and VIRGO detectors

The PSD research is essential to finding the illusive GWs. A torch illuminates the darkness, symbolising our capacity to view and understand the astonishing happenings in our universe.

The PSD plays a crucial role in the computation of parameters associated with the manifestation of GWs. The use of this technique facilitates the formulation of a "likelihood function,3.2" which ascertains the probability of witnessing the supplied data under a certain set of parameters. In a concise manner, the PSD has an impact on the allocation of weight to certain frequency components during the computation of probability.

To work with all of this, specialised information is needed: gravitational wave strain data and PSD determination for the detectors that will be utilised. Several additional elements also come into play. The "roll-off duration" is the time it takes for the data window's edges to move smoothly. It acts as a buffer to prevent unexpected consequences when analysing data, similar to padding to prevent distortion.

The "analysis segment duration" is the time spent evaluating data. Longer time periods give more information but may hinder analysis. Finally, the

"post-trigger duration" is the period after an event is noticed. Studying data after an incident prevents the bustle that follows a discovery.

To get an accurate PSD estimate that captures noise characteristics across various frequencies, examine the window and Fast Fourier Transform (FFT) parameters. These properties enable interferometer data processing for waveform modelling, likelihood calculations, and parameter estimation. All these research try to characterise the binary black hole system that caused the Gravitational-wave event.

Chapter 3

Methodology

3.1 Statistics

This chapter examines the approach for determining binary black hole parameters using gravitational wave data. This strategy relies on statistical notions. These statistical methods are important because they can extract accurate and relevant data from observable data. The next part explains fundamental statistical ideas crucial to this dissertation's analytical approach.

Mean: It is the average of many numbers. Adding them all together and dividing by the number of them gives a typical value.
Mode: It is the most frequently occurring number in the set of values. It appears to be the most noticeable.
Average: It's like mean. It's comparable to what was expected.
Peak: It's analogous to the highest point of a slope. It's where the data is most dense. It is examined to check where it is in the middle and where the data is concentrated. Finding the values that best fit the data is important.
Confidence intervals: The correct answer is likely among the following numbers. Suppose we have a 95% confidence interval. The sample process suggests that 95 out of 100 times, the correct answer will fall inside this

range. People may say, "We posit that the solution likely lies within this interval, although our certainty is not absolute."
Compatibility with Results We select the mean over the peak because it includes all values, whereas the peak may only comprise a few outstanding ones. Data that is noisy or uncommon may affect the peak. A balanced view is the mean. Confidence intervals let us assess our assumptions' confidence. The range of possible responses includes all alternatives.

These metrics aid in comprehending the data. They tell what values are frequent, where the data is more dense, and how confident the replies are. These notions, particularly when applied to the intricate task of interpreting gravitational wave phenomena, facilitate the management of ambiguity and facilitate the attainment of a more lucid comprehension.

3.2 Bayesian inference

Bayesian inference is a key methodology in statistical analysis that is based on Bayes' rule, a crucial theorem in the field of probability theory. Bayes' theorem offers a framework for revising the likelihood of a hypothesis in light of new data, making it a powerful tool for the estimation of unknown parameters. Bayesian inference is fundamentally centred on the use of Bayes' theorem:

$$p(\lambda|D) \propto p(D|\lambda) \cdot p(\lambda)[14] \tag{3.1}$$

In this equation, λ denotes a set of parameters of interest, while D represents the available data. The expression p(λ|D) signifies the posterior probability, which is the probability of λ given the data. On the other hand, p(D| λ) represents the likelihood, which quantifies the probability of observing the data given a specific λ. Lastly, p(λ) stands for the prior, indicating the initial probability assigned to λ before incorporating new data.

To better comprehend "Prior" and "Likelihood," let's examine them in Bayesian Inference.

Prior: The word "prior" pertains to a methodology for characterising the anticipated values of several characteristics associated with the binary black hole system that gave rise to the observed gravitational wave phenomenon. These attributes include characteristics such as the masses, spins, and distances of the system. Plausible or probable values may be assigned to any of these parameters within a certain range. This range is established by the use of historical data or theoretical forecasts.

The ranges associated with each parameter are formally recorded as "prior distributions." These distributions provide as a theoretical foundation for the estimation of parameters. The personnel engaged in this process ensure that the objectives they are striving for are consistent with the existing understanding of the characteristics of the system.

Within the framework of Bayesian analysis, the prior distribution is integrated with the "likelihood" function, which quantifies the degree of concordance between the available data and the underlying hypothesis. The amalgamation of these elements yields the "posterior distribution." The aforementioned distribution bears resemblance to a revised conceptual framework, including both available empirical data and initial suppositions.

The aforementioned method guides us towards the parameter values that are deemed most probable, taking into account both the observed data and our original assumptions. Understanding events becomes crucial while trying to comprehend their significance. By using this approach, we may enhance the accuracy and knowledge of our assessments pertaining to the actual values of the parameters.

Likelihood: The term "likelihood" refers to a statistical method used to compare the waveform generator's anticipated gravitational wave signal to the detectors' observed data during the event. Quantifying the agreement between model parameters and data characteristics is this method. Under

the premise that model parameters are correct, this formula quantifies the chance of seeing the data.

In order to assess the probability, a combination of many inputs is used, The academic analysis incorporates many sources of information, such as data collected from interferometers, predictions made from the waveform generator, prior distributions for the parameters (often known as priors), and requirements for Bayesian marginalisation over time, phase, and distance. The main goal of the parameter estimation methodology is to determine the ideal values for the parameters that best fit with both the model and the available data. This aim is accomplished by the calculation of probability across various parameter values. The work at hand is doing a thorough analysis of all potential parameter values in order to determine the ones that are most likely to explain the observed gravitational wave signals.

Probability is important in statistical analysis because it lets researchers compare model projections to empirical facts. Parameter values must be correctly identified to represent the physical elements of the binary black hole system that caused the gravitational event. This is done by studying GWs.

3.3 Sampling

Sampling involves picking and evaluating numerous solutions to a problem to find the best ones. The approach involves making many hypotheses on the binary black hole system that causes gravity. These attributes may include system-specific factors like masses and lengths. The goal of this effort is to find parameter values that match gravitational wave detector data.

In academia, "sampling" is systematically evaluating a variety of ideas or alternatives to find the best one. This revelation revolutionises our knowledge of the black hole system and gravitational dynamics.

3.3.1 Markov Chain Monte-Carlo

Markov Chain Monte Carlo (MCMC) sampling is a widely used technique in the field of statistical analysis. The aforementioned computational technique is used for the purpose of comprehending the distributions of samples. It is possible to comprehend the distribution of a sample without any knowledge of its mathematical features. The nomenclature "Markov Chain and Monte-Carlo" conveys two distinct concepts[15].

According to the Monte-Carlo approach, when dealing with a vast distribution, it becomes challenging to accurately determine statistics such as the mean, median, and others. In the given circumstance, a substantial quantity of samples is selected from the normal distribution[16], and afterwards, statistical calculations are performed on these data in lieu of other methodologies. In this manner, we may assess their use of it.

Based on the premise of Markov chain theory, the random samples in this particular case were generated in compliance with the predetermined requirements. Nevertheless, it is crucial to acknowledge that the upcoming sample is only contingent on the present sample, rather than the whole prior collection of created samples. Consequently, a link was being made between the two entities.

MCMC is widely recognised as a powerful computational technique in the field of Bayesian inference. This is mostly attributed to its inherent capability to successfully handle posterior distributions, which are sometimes challenging to modify using traditional analytical approaches. In the given circumstances, the use of MCMC may be employed for the estimation of the parameters pertaining to the posterior distribution, including posterior means and posterior random samples. The act of revising an initial set of beliefs to a revised set of beliefs, depending on a given set of parameters, is achieved by the utilisation of seen evidence, which is measured in terms of probability.

MCMC is a computer technique for evaluating several options. The pro-

cedure begins with well-informed assumptions that are refined to get optimal outcomes. This may be an attempt to study and evaluate different parameter selections. The validity of each assumption is assessed by comparing it against empirical evidence using "likelihood." This statistic measures the matching between expected and actual values. As sample and analysis frequency increases, most probable estimates become clearer.

3.3.2 Dynesty sampler

One of the implementation of MCMC for Gravitational wave parameter estismation is the "Dynesty" sampler from Bilby: "a user-friendly Bayesian inference library"[17]. In order to acquire knowledge on cosmic phenomena such as binary black hole collisions, a systematic methodology is required to extract relevant parameters from the available data on gravitational wave strain. The Dynesty sampler was used in this procedure for the purpose of conducting statistical analysis and estimating parameters like masses, spins, and distances.

The suggested approach integrates nested and MCMC sampling into a bespoke sampler. This technique seeks to explain Gravitational Wave origins. Nested sampling initialises a few locations in parameter space as the estimate hypothesis. These data points are enhanced by repeated refining, revealing more feasible values. In contrast, MCMC determines values by switching across parameter space areas.

The salient feature of this sampler and its approach is in its ability to effectively choose the suitable moments to include more data points and when to shift focus towards investigating alternate parameter spaces. In order to achieve thorough estimation in all possible ways. In the process of parameter space exploration using the "Dynesty" method, the primary aim is to discern the optimal correspondences between the observed strain data and the probable parameter configurations. Instead of giving precedence to exact answers, this methodology use a set of reasonable values to clarify the

characteristics and properties of the gravitational wave linked to the partial-cosmic event.

The study of GWs, particularly in relation to significant cosmic occurrences such as the GW150914 event, has considerable importance in comprehending their distinctive properties. This event, which marked the first identification of a collision between two black holes in a binary system, exemplifies the significance of such investigations. This approach helps researchers navigate the intricate process of parameter estimation through a strategic integration of thorough investigation and bold conjectures.

Chapter 4

Analysis

One of the primary goals of analysing the collected signal is to discover the intrinsic properties of a specific astronomical object i.e BBHs. This requires extracting relevant information straight from the transmission. For example, it entails measuring the distance to the source and identifying the masses of the items involved in the collision. It's worth mentioning that things with more mass produce shorter but more pronounced signals in terms of intensity.

Among the fundamental variables investigated, the chirp mass (also known as $\mathcal{M}$) stands out as a parameter that can be measured with amazing accuracy. The consideration also extends to the alignment of spin orientations with the orbital angular momentum of the object. Such alignments have an effect on the length of the signal; aligned spins provide longer signals. Orthogonal spin components, on the other hand, add to the precision of measurements inside the orbital plane and impact the amplitude and phase modulation of the signal.

The masses and spins of the objects play a crucial role in determining their significance. They provide a means to examine the historical events that precipitated the formation of merging BBHs. These characteristics provide a significant perspective on the factors that influenced the establishment and eventual consolidation of these dual systems.

When attempting to ascertain the source of a signal, two fundamental factors are taken into account: the duration it takes for the signal to reach the detector and the intensity of the signal, which is evaluated using a collection of detectors. The aforementioned detectors' measurements of the signal's strength are also considered. The importance of this matter lies in the diverse degrees of sensitivity shown by detectors in relation to the source of the signal. By doing an examination of signal intensities derived from several detectors, it becomes possible to proficiently restrict the probable orientations of the source. The procedure involves consolidating data acquired from several detectors to provide a spatial depiction that identifies the most likely position of the source inside a two-dimensional plane.

This information is critical to the event's observation. It provides a precise method for determining the specific direction from which the signal originates. In essence, this method offers a clear indicator of where the signal is genuinely originating from, considerably improving our comprehension of the astronomical event under consideration.

4.1 Source parameters characterising signals

To acquire a thorough picture of the cosmic event involving BBHs, a total of 15 parameters related to these pairs of black holes must be determined. These characteristics are useful in determining the specifics and distinguishing features of the event at issue and are briefly described below, along with their units:

Mass_1 (m1): The mass of a heavier black hole is considered primary, measured in solar masses.
Mass_2 (m2): The mass of a lighter black hole considered secondary is measured in solar masses.
Right Ascension (ra) & Declination (dec): The right ascension and

declination of the source help in identifying its location in space, measured in radians.

costheta_jn (θ_{jn}): The cosine of the angle between the line of sight and the total angular momentum vector of the system. This angle provides insight into the orientation of the system.

spin1 (a_1), costilt1 (θ_1): Primary (heavier) black hole spin magnitude (dimensionless) and cosine of the zenith angle between the spin and the orbital angular momentum vector of the system. These helps to characterise the primary black hole's rotation.

spin2 (a_2), costilt2 (θ_2): Secondary (lighter) black hole spin magnitude (dimensionless) and cosine of the zenith angle between the spin and the orbital angular momentum vector of the system. These help to characterise the secondary black hole's rotation.

luminosity_distance: It indicates how far away the source is based on the observed brightness, measured in Mpc.

chirp mass ($\mathcal{M}$) and mass ratio (q): It is a compact binary system that determines the leading-order orbital evolution of the system as a result of energy loss from emitting GWs [18].

$$\mathcal{M} = \frac{(m_1 \cdot m_2)^{3/5}}{(m_1 + m_2)^{1/5}} [19] \tag{4.1}$$

$$q = \frac{m_2}{m_1} [20] \tag{4.2}$$

nlive: It represents the number of active sets of points in the parameters during the sampling process and shows the number of live points to be examined by the sampler. The greater the number of points to be evaluated, the better the outcomes, but the greater the computing cost.

walks: The number of independent walkers that can be utilised in the sample procedure is specified by walks. Each one represents a unique chain of

samples that identify the parameters. Similarly, increasing the number of walks leads to a higher estimate but increases the cost of calculation.
n_check_point: It specifies how frequently the sampler stores checkpoint files throughout the sampling procedure. These are interim findings that can be used to restart sampling at a certain point.

Three types of analysis were being done on GWs to estimate the parameters of the various events and were classified as below:

4.2 Analysing GW150914 with various parameter estimation settings

During the investigation of the GW150914 event, a comprehensive analysis was conducted using many injection scenarios, each characterised by its unique set of setting. The examination of these parameters is of utmost importance. When investigating the vast range of possible parameter combinations and ascertaining the parameter values that are most probable.

The investigation also examined several variables, such as q, $\mathcal{M}$, a_1, a_2, θ_1, θ_2, ϕ_{12}, ϕ_{jl}, *dec*, *ra*, θ_{jn}, ψ, and time_jitter. The aforementioned parameters were thoroughly investigated through out several iterations of the investigation. The duration of analysis for each experiment showed significant variation, spanning from 2 to 96 hours.

4.3 Analysing injections of GWs similar to GW150914 into O1, O2 and O3

This study explores Compact Binary Coalescence (CBC) signals, with a particular emphasis on the collision of two black holes inside a binary system. This research project consisted of many observation sessions, namely O1, O2, and O3. The following is a summary of the methodology used for doing the

analysis:

The process started with the careful and systematic arrangement of data. The task included the determination of the time interval and sampling rate for the specific data segment in which the signal was introduced. Additionally, measures were taken to assure the replicability of the findings by creating a random seed.

The essential aspect of the study was the injection of a binary black hole waveform into the selected data segment. In order to do this, a parameter dictionary was constructed that contained essential waveform parameters. The variables of significance included in the study were the masses of the two black holes, denoted as *m1* and *m2*, together with the spins of both BBHs, represented by a tilt, and ϕ, among other pertinent factors. Additionally, the inclusion of certain predetermined variables was taken into account.

To derive valuable insights from the data, it's essential to generate waveforms. Employing an 'lal_binary_black_hole'[21] source function effectively converted specific parameters into usable waveform data. In order to efficiently detect gravity wave signals, three interferometers were used, namely LIGO-Hanford (H1), LIGO-Livingston (L1), and Virgo (V1). The objects functioned at the sensitivity levels at which they were intended. In this research, we used conventional BBH priors and a particular temporal prior that was characterised as evenly distributed around the injected value.

The major focus should be on essential factors. To optimise the efficacy of the investigation, specific attention was given to key parameters, particularly the chirp mass and mass ratio. The choices made were affected by the favourable characteristics of the respective posterior probability distributions.

By integrating interferometer data (IFOs) and the waveform generator into the likelihood function. Additionally, the concept of specified priors was introduced. In order to achieve more efficient convergence, explicit marginalisations were used for the variables of time, distance, and phase.

Consequently, the parameters of interest were obtained through a conversion function.

The dynesty sampler was used for the sampling process in this investigation. One crucial modification was the augmentation of the "maxmcmc" parameter. This facilitated the exploration of the parameter space to a greater extent throughout the rounds of the layered sampler technique.

After the completion of the sampling procedure, the conversion function assumed a crucial role in the estimation of the posterior probabilities for distance, phase, and coalescence time.

In essence, the process of analysis entails a comprehensive investigation of the estimate of parameters pertaining to continuous-wave signals. This statement highlights the significance of meticulous data setup and systematic execution when aiming to achieve an exact parameter estimate in the context of gravitational wave occurrences.

4.4 Simulating and analysing GW signals in a future network of detectors

This analysis demonstrates the procedure for injecting gravitational wave signals into a pre-existing network of detectors, occurring in the future relative to the Earth's centre and with different frequency ranges. The obtained findings provide significant insights into the estimated parameters of the injected gravitational wave signals.

The data segment duration, set at 4 seconds, and the sampling frequency, fixed at 2048 Hz, are established to facilitate the injection of the gravitational wave signal. Furthermore, the establishment of a random seed is used to ensure the reproducibility of the outcomes.

The PSD data used in this study includes the data from the Advanced Virgo detector, referred to as 'AdV_psd', as well as the detectors located at Hanford and Livingston, denoted as 'aLIGO_ZERO_DET_high_P_psd'. The

PSDs have been subjected to a filtering process in order to retain only those frequencies that are equal to or greater than mentioned ones.

The concept of frequency range refers to the span of frequencies inside a given system or phenomenon. It encompasses the lowest and highest frequencies that may be detected or transmitted within that system. A frequency array is created, covering a range of 1 Hz to 1000 Hz, consisting of 1000 data points.

The configuration of interferometers entails the meticulous modification and calibration of several components in order to enhance their performance and guarantee precise results. The interferometers are designed to match the Hanford (H1), Livingston (L1), and Virgo (V1) locations. The arguments put forth in support of the waveform model have been addressed and resolved. The waveform approximant used for this study is 'IMRPhenomPv2,' with the reference frequency specified as 50 Hz.

A waveform generator is developed by using the 'lal_binary_black_hole'[21] source function. The key factors included in this study consist of the duration, sampling frequency, frequency domain source model, and waveform arguments. The prior distributions for different parameters are established mostly based on the injection parameters.

Integrating the interferometer data, waveform generator, and predefined priors results in the initialization of the probability. This encompasses the process of marginalisation across many dimensions such as time, phase, and distance, along with the integration of past knowledge.

The parameter space is investigated using the 'dynesty' sampler. The setup choices include live points, walkers, checkpoint intervals, and log-likelihood increment. The conversion function estimates distance, phase, and coalescence time posterior probabilities after processing. The source code for this study is here: https://github.com/VudayagiriDhruv/MTHM038---Project-Dissertation-tree/main/code

Chapter 5

Results

5.1 GW150914 with different parameter estimation settings

In this section, the focus shifts to the presentation of outcomes from the analysis. The investigation centers around the event GW150914, and the exploration of its behavior under various parameter estimation settings is the primary objective 4.2.

The study included two distinct operating modes, namely Terminal and Jupyter, with adjustments made to key parameters like nlive, walks, n_check_point, and dlogz. The findings of this study have some noteworthy implications.

Comparison of run modes: The Terminal and Jupyter operating modes allowed results and effectiveness analysis in these contexts. The analytical procedure's efficiency and effectiveness depend on this selection.

The sensitivity of parameter exploration: Modifying the setup parameters, namely nlive, walks, n_check_point, and dlogz, significantly influenced the parameter estimation process. The selection of appropriate values for these characteristics is of utmost importance since they have the potential to greatly impact the outcomes of the study.

Variability in the estimation of mass ratios: The determination of the mass

Table 5.1: Results for GW150914 injections

Run	1	2	3	4	5	6
Run Mode	Terminal	Jupyter	Jupyter	Terminal	Terminal	Jupyter
nlive	1000	1000	256	256	256	256
walks	100	100	50	50	100	100
n check point	10000	10000	5000	5000	5000	5000
dlogz	0.10	0.10	0.50	0.50	0.25	0.25
mass_ratio	$0.86^{+0.10}_{-0.13}$	$0.86^{+0.10}_{-0.12}$	$0.86^{+0.09}_{-0.12}$	$0.86^{+0.09}_{-0.13}$	$0.86^{+0.10}_{-0.13}$	$0.86^{+0.09}_{-0.12}$
chirp_mass	$30.86^{+0.85}_{-0.85}$	$30.66^{+0.83}_{-0.89}$	$30.66^{+0.81}_{-0.76}$	$30.60^{+0.89}_{-0.80}$	$30.65^{+0.82}_{-0.91}$	$30.68^{+0.86}_{-0.83}$
a_1	$0.29^{+0.36}_{-0.21}$	$0.29^{+0.36}_{-0.21}$	$0.30^{+0.37}_{-0.21}$	$0.29^{+0.34}_{-0.20}$	$0.30^{+0.35}_{-0.22}$	$0.28^{+0.36}_{-0.21}$
a_2	$0.34^{+0.37}_{-0.23}$	$0.35^{+0.37}_{-0.24}$	$0.34^{+0.36}_{-0.23}$	$0.34^{+0.37}_{-0.23}$	$0.34^{+0.38}_{-0.25}$	$0.36^{+0.33}_{-0.26}$
tilt_1	$1.7^{+0.58}_{-0.63}$	$1.69^{+0.61}_{-0.63}$	$1.71^{+0.54}_{-0.70}$	$1.68^{+0.56}_{-0.65}$	$1.73^{+0.60}_{-0.71}$	$1.68^{+0.55}_{-0.64}$
tilt_2	$1.78^{+0.60}_{-0.65}$	$1.79^{+0.57}_{-0.64}$	$1.79^{+0.56}_{-0.71}$	$1.78^{+0.60}_{-0.59}$	$1.79^{+0.59}_{-0.63}$	$1.78^{+0.57}_{-0.61}$
phi_12	$3.11^{+2.15}_{-2.11}$	$3.11^{+2.12}_{-2.14}$	$3.19^{+2.07}_{-2.11}$	$3.17^{+2.18}_{-2.07}$	$3.12^{+2.17}_{-2.17}$	$3.08^{+2.18}_{-2.02}$
phi_jl	$3.17^{+2.02}_{-2.23}$	$3.02^{+2.14}_{-2.13}$	$3.31^{+1.93}_{-2.48}$	$3.18^{+2.07}_{-2.21}$	$3.03^{+2.16}_{-2.21}$	$3.02^{+2.07}_{-2.09}$
dec	$-1.21^{+0.12}_{-0.05}$	$-1.21^{+0.12}_{-0.05}$	$-1.22^{+0.10}_{-0.05}$	$-1.2^{+0.12}_{-0.06}$	$-1.21^{+0.11}_{-0.05}$	$-1.21^{+0.12}_{-0.05}$
ra	$2.02^{+0.46}_{-0.75}$	$2.04^{+0.46}_{-0.73}$	$2.09^{+0.38}_{-0.76}$	$2.06^{+0.43}_{-0.80}$	$2.04^{+0.45}_{-0.78}$	$2.03^{+0.47}_{-0.71}$
theta_jn	$2.72^{+0.23}_{-0.42}$	$2.72^{+0.23}_{-0.40}$	$2.74^{+0.21}_{-0.32}$	$2.72^{+0.24}_{-0.49}$	$2.73^{+0.23}_{-0.41}$	$2.70^{+0.24}_{-0.42}$
psi	$1.54^{+1.08}_{-1.08}$	$1.58^{+1.08}_{-1.05}$	$1.58^{+1.05}_{-1.10}$	$1.61^{+1.02}_{-1.13}$	$1.50^{+1.09}_{-1.05}$	$1.49^{+1.04}_{-1.05}$
time_jitter	$0^{+0.0}_{-0.0}$	$0^{+0.0}_{-0.0}$	$0^{+0.0}_{-0.0}$	$0^{+0.0}_{-0.0}$	$0^{+0.0}_{-0.0}$	$0^{+0.0}_{-0.0}$
Duration (hrs)	48	96	5	2.19	6.28	17

ratio for the GW150914 event has significant importance. A central value of 0.86 was identified; nevertheless, there is a degree of ambiguity associated with this number. It is worth noting that the selection of the run mode and the individual parameter combinations had a significant impact on these estimations.

The dynamics of the chirp mass: The chirp mass estimates exhibited a range spanning from 30.60 to 30.86, accompanied by a degree of uncertainty. This demonstrates that the manner in which the study is established, including the selection of run mode and parameters, has an impact on the estimations of the chirp mass.
Sensitivity of spin parameters: The parameters denoting the rotational properties of black holes, namely a_1, and a_2, exhibited notable fluctuations across many iterations and configurations. This underscores the susceptibility of these characteristics to the specific analytic settings used.
Variations in tilt and phase angle: The estimated values of the tilt angles (θ_1 and θ_2) and the phase parameters (ϕ_{12} and ϕ_{jl}) exhibited substantial differences in the context of describing the tilting characteristics of black holes. This observation indicates that the selection of run mode and setup settings has a substantial impact on the values of these angles.
Sensitivity to sky position and orientation: The variations in parameters pertaining to the celestial position of a source, such as *dec* and *ra*, exhibited minor discrepancies across different experimental runs and observational modes. Moreover, the orientation angles, such as θ_{jn} and ψ, were subject to the impact of analysis parameters.
Time jitter consistency: The term "time jitter consistency" refers to the extent of variability or lack of uniformity in the temporal sequencing of occurrences or signals. This applies to the regularity and predictability of temporal phenomena. The temporal jitter parameter had consistent behaviour across all experimental runs and modes, suggesting that it was hardly affected by variations in setup configurations.
Analysis duration: The analysis duration refers to the length of time required to conduct an analysis. Finally, the duration of the analysis ranged from 2.19 hours to 96 hours. The primary factor that drove this was the processing resources required for various setups. The significance of work on GW150914 lies in the recognition of the criticality of selecting appropriate setup parameters, run modes, and settings during the estimation of parameters from gravitational wave data.

5.2 Results for analysing injections of GWs similar to GW150914 into O1, O2 and O3

Two sets of gravitational wave injections had been studied: one from O2 (detectors H1 and L1 as well as V1 for some events), and the other from O3 (detectors H1, L1, and V1). The interesting thing that has been found is that the uncertainties for the parameters in each gravitational event have their own unique value, emphasising the need for careful analysis of every event. To handle uncertainties in measurements, asymmetric error bars were used. These bars include both upper and lower error values, which accurately capture the uneven nature of uncertainty. This method gives a complete picture of the possible range of each parameter measurement, acknowledging that error can vary in different directions.

5.2.1 O2 with H1 and L1 detectors: gravitational wave property variation results

To analyse the factors contributing to the observed variations in gravitational wave trends and their association with distinct attributes of the discovered binary black hole systems in O2 run.

Mass ratios: The observed range of mass ratios (0.67 to 0.85) may be attributed to the intrinsic heterogeneity present within these binary systems. A larger value of q indicates a significant disparity in the mass between the two black holes. The observed variety may be attributed to disparities in the formation and evolution processes of these binary systems. As an example, the event GW170809, characterised by a q value of 0.85, implies the presence of a binary system including a primary black hole of much greater mass.

Chirp mass: The variation in chirp masses (ranging from 27.37 to 28.25) indicates disparities in the combined mass of the binary system. The aforementioned parameter is subject to the impact of both the masses of black holes and their orbital dynamics. A decreased chirp mass corresponds to a reduced mass of the binary system. The observed variances in these binaries may be attributed to differences in their creation history. As an example, the event GW170104 has a

Parameters	input	Injection	Injection	Injection	input	Injection	Injection	Injection	Injection	Injection
Detectors		H1, L1	H1, L1	H1, L1	H1, L1	H1, L1	H1, L1	H1, L1	H1, L1	H1, L1
Event		GW170104	GW170608	GW170729	GW170809	GW170814	GW170817	GW170818	GW170823	GW190408_181802
geocent_time		1167560116	1180922674	1185389987	1186302699	1186742041	1187009062	1187058507	1187529436	1238782880
nlive		512	512	512	512	512	512	512	512	512
walks		100	100	100	100	100	100	100	100	100
n_check_point		5000	5000	5000	5000	5000	5000	5000	5000	5000
dlogz		0.2	0.2	0.2	0.2	0.2	0.2	0.2	0.2	0.2
q	0.8	$0.75^{+0.17}_{-0.16}$	$0.67^{+0.19}_{-0.11}$	$0.78^{+0.15}_{-0.16}$	$0.85^{+0.11}_{-0.14}$	$0.80^{+0.14}_{-0.17}$	$0.80^{+0.13}_{-0.16}$	$0.74^{+0.17}_{-0.14}$	$0.81^{+0.13}_{-0.16}$	$0.70^{+0.20}_{-0.14}$
chirpmass	28.09	$27.37^{+0.86}_{-0.86}$	$28.22^{+0.62}_{-0.65}$	$27.88^{+1.04}_{-1.00}$	$28.07^{+0.56}_{-0.57}$	$27.51^{+0.64}_{-0.63}$	$27.56^{+0.76}_{-0.78}$	$28.25^{+0.59}_{-0.57}$	$27.43^{+0.82}_{-0.79}$	$27.75^{+0.70}_{-0.66}$
mass_1	36	36.38	39.76	36.32	35.00	35.37	35.44	37.81	35.05	38.22
mass_2	29	27.28	26.64	28.33	29.75	28.30	28.35	27.98	28.39	26.75
a_1	0.40	$0.42^{+0.29}_{-0.26}$	$0.58^{+0.22}_{-0.28}$	$0.51^{+0.28}_{-0.29}$	$0.61^{+0.25}_{-0.30}$	$0.45^{+0.29}_{-0.27}$	$0.48^{+0.27}_{-0.30}$	$0.48^{+0.25}_{-0.28}$	$0.46^{+0.31}_{-0.30}$	$0.44^{+0.26}_{-0.27}$
a_2	0.30	$0.52^{+0.30}_{-0.32}$	$0.57^{+0.28}_{-0.36}$	$0.52^{+0.30}_{-0.34}$	$0.49^{+0.30}_{-0.32}$	$0.51^{+0.31}_{-0.32}$	$0.48^{+0.31}_{-0.31}$	$0.54^{+0.29}_{-0.34}$	$0.50^{+0.31}_{-0.32}$	$0.53^{+0.31}_{-0.33}$
tilt_1	0.50	$1.02^{+0.63}_{-0.49}$	$0.93^{+0.41}_{-0.37}$	$0.95^{+0.58}_{-0.46}$	$0.83^{+0.47}_{-0.38}$	$1.02^{+0.59}_{-0.44}$	$0.98^{+0.55}_{-0.46}$	$0.87^{+0.59}_{-0.41}$	$1.03^{+0.57}_{-0.49}$	$0.91^{+0.58}_{-0.43}$
tilt_2	1.00	$1.05^{+0.74}_{-0.50}$	$1.03^{+0.65}_{-0.46}$	$1.09^{+0.77}_{-0.53}$	$1.19^{+0.71}_{-0.61}$	$1.11^{+0.70}_{-0.53}$	$1.17^{+0.72}_{-0.59}$	$0.94^{+0.75}_{-0.46}$	$1.19^{+0.71}_{-0.55}$	$0.98^{+0.73}_{-0.49}$
phi_12	1.70	$3.17^{+2.14}_{-2.26}$	$3.19^{+2.16}_{-2.26}$	$3.11^{+2.12}_{-2.06}$	$3.16^{+2.25}_{-2.24}$	$3.22^{+2.04}_{-2.19}$	$3.12^{+2.12}_{-2.07}$	$3.17^{+2.06}_{-2.23}$	$3.10^{+2.20}_{-2.10}$	$3.08^{+2.13}_{-2.11}$
phi_jl	0.30	$2.03^{+2.49}_{-2.04}$	$3.44^{+0.77}_{-2.78}$	$2.87^{+2.24}_{-1.69}$	$3.16^{+2.25}_{-2.24}$	$3.17^{+2.43}_{-2.16}$	$3.10^{+2.09}_{-2.10}$	$3.24^{+2.39}_{-2.53}$	$3.18^{+2.03}_{-2.17}$	$2.93^{+2.32}_{-2.07}$
theta_jn	0.40	$2.29^{+0.49}_{-1.61}$	$1.94^{+0.58}_{-1.29}$	$2.26^{+0.53}_{-1.62}$	$0.62^{+1.78}_{-0.35}$	$1.04^{+1.56}_{-0.65}$	$1.35^{+1.32}_{-0.94}$	$2.28^{+0.51}_{-1.79}$	$1.33^{+1.35}_{-0.93}$	$1.52^{+1.11}_{-1.04}$
psi	2.659	$1.56^{+1.04}_{-1.04}$	$1.54^{+0.96}_{-1.11}$	$1.51^{+1.08}_{-1.01}$	$1.57^{+1.12}_{-1.03}$	$1.55^{+1.13}_{-1.05}$	$1.58^{+1.13}_{-1.00}$	$1.57^{+1.02}_{-1.01}$	$1.59^{+1.11}_{-1.06}$	$1.59^{+1.15}_{-1.13}$
dec	-1.21	-0.2	-0.53	-0.28	-1.05	-1.1	-1.08	-0.67	-1.01	-1.11
ra	1.375	$5.15^{+0.48}_{-2.42}$	$4.05^{+2.05}_{-3.69}$	$4.67^{+0.45}_{-2.06}$	$1.66^{+0.12}_{-0.52}$	$2.08^{+0.25}_{-0.82}$	$2.96^{+0.13}_{-1.13}$	$0.96^{+0.5}_{-0.18}$	$3.38^{+0.07}_{-0.58}$	$1.96^{+0.23}_{-0.89}$
luminosity_distance	2000									
phase	1.30									
Duration (hrs:mins)		02:05	20:11	01:43	03:56	12:23	04:07	21:00	02:06	04:32

Figure 5.1: Injection Results for O2 run with H1,L1 detectors

comparatively modest chirp mass value of 27.37, suggesting the presence of a system with lower overall mass.

Spin properties: Disparities in spin magnitudes, such as a_1 and a_2, are plausibly associated with the distinct evolutionary trajectories of individual binary systems. The rotational properties of progenitor stars and their interactions throughout stellar development have an impact on the spins of black holes. An illustration of this may be seen in the case of GW170104, which has a reasonably significant spin magnitude a_1 of 0.42. This observation implies the presence of a black hole with considerable intrinsic angular momentum.

Orientation parameters: The changes in orientation parameters, namely tilt, ϕ_{12}, ϕ_{jl}, and θ_{jn}, are intricately linked to the beginning circumstances of these binary systems. The tilt angles are contingent upon the respective orientations of the angular momentum vectors of black holes, while ϕ_{12} and ϕ_{jl} denote the orientations of the spins of black holes and the orbital plane of the binary system. The use of numerical data, namely the examination of changes in ϕ_{12} values, provides a means to illustrate the disparities in these angles across different occurrences.

Polarization angle: The polarisation angle exhibits changes, denoted as +1.04/-1.04, that result from variations in the orientations of binary systems relative to the observer. The variations found in the merging of black holes may be ascribed to the intrinsic stochastic nature that exists within the cosmic environment. In the instance of GW170809, it is seen that the parameter ψ exhibits a numerical value of 1.57, signifying a certain orientation of the polarisation of the gravitational wave.

Sky coordinates (declination and right ascension): The spatial distribution of black hole binary systems in the celestial sphere is reflected in the changes seen in the celestial coordinates of these occurrences, specifically in terms of declination and right ascension. The observed fluctuations include a spectrum of declination values spanning from -0.20 to -1.11. Additionally, the uncertainty in right ascension for GW170104 are shown as +0.48/-2.42. The identification of these placements relies on the geographic distribution of the host galaxies and their alignment relative to Earth.

Temporal diversity: The considerable span of geocentric periods implies that

these mergers of black holes took place throughout distinct cosmic epochs. The temporal variety seen in these binary systems may be attributed to the convergence of separate evolutionary trajectories that have culminated in their genesis and subsequent merging.

The alterations in gravitational wave characteristics may be attributed to the astrophysical mechanisms that regulate the behaviour of binary black hole systems. The aforementioned processes include the initial parameters of progenitor stars, including their masses, spins, and orbital dynamics. The numerical values pertaining to these parameters provide valuable insights into the diverse nature of black hole mergers and contribute significant knowledge about the intricate astrophysical processes that influence our universe.

5.2.2 O2 with H1, L1 and V1 detectors: gravitational wave property variation results

Upon scrutinising the injection outcomes spanning from runs 1 to 9, as seen via the H1, L1 and V1 detectors, discernible patterns and enhancements in many gravitational wave properties become apparent.

Mass ratios: The estimation of mass ratios (q) exhibits a discernible pattern of enhanced accuracy as we go from earlier to subsequent experiments. The reduction in uncertainty intervals signifies an improvement in our ability to ascertain the mass ratios of the black hole binaries. In the case of GW190408_181802 event, the mass ratio is approximated as $q = 0.75^{+0.17}_{-0.15}$.

Chirp mass: The accuracy of chirp mass estimations increases as we go through the runs, similar to the improvement seen in mass ratios. This observation implies that there is an increasing level of precision in the estimation of the combined mass of these binary black hole systems. As an example, the chirp mass in GW170818 event is calculated to be $28.48^{+0.55}_{-0.57}$.

Spin properties: The uncertainty ranges for spin magnitudes exhibit a reduction in width across subsequent iterations, suggesting an improvement in the accuracy of black hole spin measurements. This contributes to the advancement of our comprehension about the angular momentum properties shown by these systems.

Parameters	input	Injection	Injection	Injection	injection	Injection	Injection	Injection	Injection	Injection
run		run1	run2	run3	run4	run5	run6	run7	run8	run9
Detectors		H1, L1	H1, L1	H1, L1, V1	H1, L1, V1	H1, L1, V1	H1, L1, V1	H1, L1, V1	H1, L1	H1, L1
Event		GW170104	GW170608	GW170729	GW170809	GW170814	GW170817	GW170818	GW170823	GW190408_181802
geocent_time		1167560116	1180922674	1185389987	1186302699	1186742041	1187009062	1187058507	1187529436	1238782880
nlive		512	512	512	512	512	512	512	512	512
walks		100	100	100	100	100	100	100	100	100
n_check_point		5000	5000	5000	5000	5000	5000	5000	5000	5000
dlogz		0.2	0.2	0.2	0.2	0.2	0.2	0.2	0.2	0.2
q	0.8	$0.75^{+0.17}_{-0.16}$	$0.67^{+0.19}_{-0.11}$	$0.77^{+0.15}_{-0.15}$	$0.83^{+0.12}_{-0.14}$	$0.81^{+0.13}_{-0.16}$	$0.79^{+0.14}_{-0.14}$	$0.77^{+0.16}_{-0.17}$	$0.84^{+0.11}_{-0.15}$	$0.75^{+0.17}_{-0.15}$
chirpmass	28.09	$27.37^{+0.86}_{-0.86}$	$28.22^{+0.62}_{-0.65}$	$27.71^{+0.79}_{-0.74}$	$27.94^{+0.56}_{-0.53}$	$27.38^{+0.55}_{-0.57}$	$27.65^{+0.64}_{-0.67}$	$28.48^{+0.55}_{-0.57}$	$27.50^{+0.62}_{-0.63}$	$27.66^{+0.58}_{-0.62}$
mass_1	36	36.38	39.76	36.34	35.26	34.98	35.78	37.35	34.49	36.76
mass_2	29	27.28	26.64	27.98	29.26	28.34	28.27	28.76	28.97	27.57
a_1	0.40	$0.42^{+0.29}_{-0.26}$	$0.58^{+0.22}_{-0.28}$	$0.48^{+0.25}_{-0.29}$	$0.58^{+0.25}_{-0.30}$	$0.44^{+0.27}_{-0.26}$	$0.44^{+0.28}_{-0.26}$	$0.54^{+0.34}_{-0.31}$	$0.45^{+0.26}_{-0.28}$	$0.44^{+0.26}_{-0.26}$
a_2	0.30	$0.52^{+0.30}_{-0.32}$	$0.57^{+0.28}_{-0.36}$	$0.51^{+0.29}_{-0.33}$	$0.48^{+0.31}_{-0.32}$	$0.48^{+0.29}_{-0.31}$	$0.47^{+0.30}_{-0.31}$	$0.57^{+0.27}_{-0.37}$	$0.47^{+0.30}_{-0.31}$	$0.50^{+0.30}_{-0.32}$
tilt_1	0.50	$1.02^{+0.63}_{-0.49}$	$0.93^{+0.41}_{-0.37}$	$0.98^{+0.59}_{-0.46}$	$0.86^{+0.49}_{-0.49}$	$1.02^{+0.57}_{-0.47}$	$0.94^{+0.64}_{-0.44}$	$0.87^{+0.51}_{-0.42}$	$0.98^{+0.63}_{-0.47}$	$0.95^{+0.58}_{-0.45}$
tilt_2	1.00	$1.05^{+0.74}_{-0.50}$	$1.03^{+0.65}_{-0.46}$	$1.12^{+0.75}_{-0.54}$	$1.15^{+0.78}_{-0.57}$	$1.16^{+0.72}_{-0.54}$	$1.10^{+0.84}_{-0.54}$	$0.97^{+0.73}_{-0.48}$	$1.14^{+0.73}_{-0.57}$	$1.02^{+0.74}_{-0.51}$
phi_12	1.70	$3.17^{+2.14}_{-2.26}$	$3.19^{+2.16}_{-2.26}$	$3.16^{+2.10}_{-2.18}$	$3.15^{+2.21}_{-2.10}$	$3.21^{+2.08}_{-2.19}$	$3.15^{+2.17}_{-2.19}$	$3.20^{+2.14}_{-2.05}$	$3.06^{+2.18}_{-2.06}$	$3.09^{+2.16}_{-2.15}$
phi_jl	0.30	$2.03^{+2.49}_{-2.04}$	$3.44^{+0.77}_{-2.78}$	$4.85^{+0.83}_{-1.86}$	$2.62^{+3.20}_{-2.10}$	$4.65^{+0.97}_{-3.17}$	$2.77^{+2.31}_{-2.00}$	$2.76^{+0.86}_{-0.84}$	$3.26^{+2.20}_{-2.48}$	$4.32^{+1.45}_{-3.53}$
theta_jn	0.40	$2.29^{+0.49}_{-1.61}$	$1.94^{+0.58}_{-1.29}$	$0.58^{+0.37}_{-0.27}$	$0.50^{+0.42}_{-0.26}$	$0.66^{+0.75}_{-0.32}$	$0.91^{+1.69}_{-0.56}$	$0.51^{+0.28}_{-0.25}$	$0.62^{+0.99}_{-0.35}$	$0.67^{+0.88}_{-0.35}$
psi	2.659	$1.56^{+1.04}_{-1.04}$	$1.54^{+0.96}_{-1.11}$	$1.54^{+1.23}_{-0.93}$	$1.56^{+1.04}_{-1.15}$	$1.59^{+0.97}_{-1.02}$	$1.56^{+1.23}_{-0.99}$	$1.57^{+1.11}_{-1.03}$	$1.59^{+1.13}_{-1.13}$	$1.58^{+0.94}_{-1.08}$
dec	-1.21	-0.2	-0.53	-1.2	-1.2	-1.21	-1.22	-1.21	-1.21	-1.22
ra	1.375	$5.15^{+0.48}_{-2.42}$	$4.05^{+2.05}_{-3.69}$	$1.35^{+0.06}_{-0.06}$	$1.36^{+0.04}_{-0.04}$	$1.38^{+0.02}_{-0.02}$	$1.39^{+0.05}_{-0.07}$	$1.39^{+0.03}_{-0.03}$	$1.40^{+0.05}_{-0.06}$	$1.38^{+0.05}_{-0.02}$
phase	1.30									
luminosity_distance	2000									
Duration (hrs:mins)		02:05	20:11	03:25	19:24	20:39	25.2	28.48	2.57	14.47

Figure 5.2: Injection Results for O2 run with H1,L1,V1 detectors

As an example, in GW170818 event, the value of a_1 is calculated to be $0.54^{+0.34}_{-0.31}$, whereas the value of a_2 is determined to be $0.57^{+0.27}_{-0.37}$.

Orientation parameters: The orientation parameters, including tilt, ϕ_{12}, ϕ_{jl}, and θ_{jn}, are being considered. The presence of fluctuations in orientation parameters seen over several runs highlights the advancements made in accurately characterising the orientation of binary systems. The aforementioned enhancements are evident in the reduced width of the uncertainty intervals pertaining to parameters such as tilt angles and azimuthal angles. In the eight iteration of the run i.e GW170823, the estimated value for $\tilde{a}_1$ is 0.98 with an upper uncertainty of 0.63 and a lower uncertainty of -0.47. Similarly, the projected value for ϕ_{jl} is 3.26 with an upper uncertainty of 2.20 and a lower uncertainty of -2.48.

Polarization angle: The precision of predicting polarisation angle values improves with each iteration. This enables a more precise assessment of the polarisation characteristics of gravitational waves. As an example, for GW190408_181802 event, the estimated value of ψ is determined to be 1.58 with a confidence interval of 0.94 to -1.08.

Sky coordinates (declination and right ascension): The celestial coordinates, namely the declination and right ascension, exhibit a degree of stability throughout time. However, subsequent observations have yielded minor enhancements in the accuracy of location estimates. In the case of run9, the declination is recorded as -1.22, while the right ascension is approximated as $1.38^{+0.05}_{-0.02}$.

Temporal diversity: Temporal diversity is seen in gravitational wave events, since the length of these events exhibits variation between different runs. Notably, later runs tend to have larger durations compared to earlier ones. This suggests advancements in the ability to capture signals that have a longer duration. In the Run7 simulation, the length is projected to be around 28:48 hours.

In summary, as we go through the iterations, a discernible pattern emerges whereby the accuracy of predicting crucial gravitational wave characteristics exhibits consistent improvement. The aforementioned changes significantly improve our capacity to accurately characterise binary black hole systems, hence making a substantial contribution towards a more comprehensive comprehension of these astronomical phenomena.

5.2.3 O3 with H1, L1 and V1 detectors: gravitational wave property variation results

The current O3, which included the H1, L1, and V1 detectors, improved our capacity to accurately characterise gravitational wave event characteristics. The inherent differences between these events and those in the prior O2 run make it impossible to directly compare them, although the overall development may be assessed.

Enhanced precision in mass and spin measurements: The mass ratios (q) of merging black hole systems may now be determined with increased accuracy. This implies that there is an enhanced comprehension about the comparative masses of the black holes that are implicated.

The estimation of the chirp mass, a parameter that provides insights into the evolutionary trajectory of a binary system, has been refined with increased accuracy.

Enhanced spin characterization: The magnitudes of spin (a_1 and a_2) have shown advancements in their measurement techniques for black holes within the context of gravitational wave occurrences. This observation helps our comprehension of the rotational velocity of these entities.

Expanded orientation information: The accuracy of tilt angle measurements has been enhanced for $\tilde{a}_1$ and $\tilde{a}_2$. This implies that a more comprehensive comprehension of the orientation of these black hole systems may be attained.

The precision of our observations pertaining to the azimuthal angle, which characterises the angular separation between the spins of the two black holes, has significantly improved.

The enhancement of sky localization: The precision of determining the celestial coordinates (namely, declination and right ascension) for gravitational wave occurrences has significantly improved. The importance of this cannot be overstated in the context of subsequent observations conducted using other telescope technologies.

The term ψ refers to a phenomena characterised by the alteration or intensification of the polarisation angle of a certain entity or system. The precision of psi measurements has been maintained or improved. This facilitates the understand-

Parameters	input	Injection	Injection	Injection	input	Injection	Injection	Injection	Injection	Injection	Injection
run		run1	run2	run3	run4	run5	run6	run7	run8	run9	run10
Detectors		H,L1,V1	H1, L1	H1,L1,V1	H1, L1	L1, V1	H1,L1	H1, L1, V1	H1, L1, V1	H1, L1, V1	H1, L1
Event		GW190412	GW190413_052954	GW190413_134308	GW190421_213856	GW190425	GW190426_190642	GW190503_185404	GW190512_180714	GW190513_205428	GW190514_065416
geocent_time		1239082442	1239168792	1239198386	1239918134	1240215683	1240341000	1240945042	1241719652	1241816266	1241852254
nlive		512	512	512	512	512	512	512	512	512	512
walks		100	100	100	100	100	100	100	100	100	100
n_check_point		5000	5000	5000	5000	5000	5000	5000	5000	5000	5000
dlogz		0.2	0.2	0.2	0.2	0.2	0.2	0.2	0.2	0.2	0.2
q	0.8	$0.67^{+0.18}_{-0.11}$	$0.68^{+0.20}_{-0.12}$	$0.68^{+0.19}_{-0.12}$	$0.81^{+0.13}_{-0.16}$	$0.82^{+0.12}_{-0.15}$	$0.80^{+0.14}_{-0.14}$	$0.83^{+0.11}_{-0.15}$	$0.84^{+0.11}_{-0.14}$	$0.74^{+0.17}_{-0.14}$	$0.86^{+0.09}_{-0.13}$
chirpmass	28.09	$27.82^{+0.53}_{-0.53}$	$27.80^{+0.60}_{-0.62}$	$28.18^{+0.52}_{-0.58}$	$27.41^{+0.68}_{-0.63}$	$28.09^{+0.59}_{-0.54}$	$27.53^{+0.65}_{-0.68}$	$27.84^{+0.58}_{-0.60}$	$27.94^{+0.58}_{-0.58}$	$27.64^{+0.71}_{-0.70}$	$27.94^{+0.50}_{-0.52}$
mass_1	36	39.20	38.87	39.40	35.02	35.67	35.40	35.13	35.04	36.99	34.63
mass_2	29	26.26	26.43	26.79	28.37	29.25	28.32	29.16	29.44	27.37	29.78
a_1	0.40	$0.41^{+0.26}_{-0.25}$	$0.50^{+0.25}_{-0.29}$	$0.49^{+0.22}_{-0.28}$	$0.43^{+0.26}_{-0.28}$	$0.66^{+0.24}_{-0.33}$	$0.50^{+0.28}_{-0.28}$	$0.52^{+0.27}_{-0.31}$	$0.55^{+0.26}_{-0.30}$	$0.43^{+0.29}_{-0.26}$	$0.63^{+0.24}_{-0.32}$
a_2	0.30	$0.55^{+0.29}_{-0.33}$	$0.56^{+0.29}_{-0.36}$	$0.51^{+0.29}_{-0.33}$	$0.46^{+0.31}_{-0.28}$	$0.53^{+0.30}_{-0.36}$	$0.50^{+0.30}_{-0.32}$	$0.48^{+0.30}_{-0.32}$	$0.49^{+0.32}_{-0.33}$	$0.49^{+0.30}_{-0.32}$	$0.54^{+0.28}_{-0.34}$
tilt_1	0.50	$0.96^{+0.63}_{-0.43}$	$0.99^{+0.48}_{-0.41}$	$0.79^{+0.51}_{-0.38}$	$0.99^{+0.62}_{-0.48}$	$0.94^{+0.43}_{-0.38}$	$0.97^{+0.55}_{-0.46}$	$0.92^{+0.54}_{-0.44}$	$0.92^{+0.50}_{-0.45}$	$0.94^{+0.62}_{-0.44}$	$0.98^{+0.47}_{-0.42}$
tilt_2	1.00	$0.93^{+0.74}_{-0.46}$	$1.05^{+0.67}_{-0.48}$	$0.97^{+0.81}_{-0.47}$	$1.11^{+0.78}_{-0.55}$	$1.19^{+0.67}_{-0.56}$	$1.20^{+0.77}_{-0.57}$	$1.13^{+0.77}_{-0.55}$	$1.15^{+0.72}_{-0.56}$	$1.06^{+0.83}_{-0.51}$	$1.19^{+0.66}_{-0.54}$
phi_12	1.70	$3.22^{+2.05}_{-2.14}$	$3.10^{+2.14}_{-2.17}$	$3.20^{+2.07}_{-2.13}$	$3.13^{+2.12}_{-2.14}$	$3.14^{+2.10}_{-2.13}$	$3.15^{+2.16}_{-2.11}$	$3.07^{+2.11}_{-2.11}$	$3.22^{+2.13}_{-2.22}$	$3.27^{+2.04}_{-2.27}$	$3.09^{+2.19}_{-2.10}$
phi_jl	0.30	$1.06^{+44.25}_{-0.71}$	$3.27^{+1.04}_{-2.58}$	$1.70^{+1.50}_{-0.90}$	$3.77^{+1.75}_{-2.84}$	$0.99^{+4.27}_{-0.63}$	$3.32^{+1.98}_{-2.05}$	$3.30^{+1.67}_{-2.17}$	$3.50^{+1.62}_{-2.16}$	$3.90^{+1.70}_{-3.14}$	$2.81^{+1.91}_{-1.97}$
theta_jn	0.40	$0.52^{+0.27}_{-0.25}$	$1.86^{+0.70}_{-1.24}$	$0.58^{+0.41}_{-0.28}$	$0.58^{+0.84}_{-0.31}$	$0.58^{+0.26}_{-0.26}$	$1.03^{+1.58}_{-0.66}$	$0.62^{+1.63}_{-0.36}$	$0.55^{+1.02}_{-0.31}$	$0.54^{+0.45}_{-0.26}$	$1.96^{+0.78}_{-1.53}$
psi	2.659	$1.55^{+1.03}_{-1.13}$	$1.57^{+1.01}_{-1.10}$	$1.57^{+1.11}_{-0.93}$	$1.57^{+1.10}_{-1.15}$	$1.54^{+1.10}_{-1.05}$	$1.58^{+1.12}_{-1.05}$	$1.56^{+1.14}_{-0.92}$	$1.59^{+1.11}_{-0.95}$	$1.55^{+1.07}_{-1.09}$	$1.53^{+1.12}_{-1.02}$
dec	-1.21	-1.21	-0.55	-1.21	-1.21	-1.11	-1.1	-1.21	-1.2	-1.21	-0.7
ra	1.375	$1.37^{+0.02}_{-0.02}$	$4.09^{+2.01}_{-3.74}$	$1.37^{+0.04}_{-0.04}$	$1.41^{+0.06}_{-0.06}$	$1.60^{+0.14}_{-0.19}$	$2.50^{+0.23}_{-0.97}$	$1.39^{+0.03}_{-0.04}$	$1.39^{+0.02}_{-0.03}$	$1.45^{+0.06}_{-0.06}$	$0.67^{+0.93}_{-0.25}$
luminosity_distance	2000										
phase	1.30										
Duration (hrs:mins)		04:22	06:54	10:56	01:58	04:52	11:19	03:05	04:36	25.04	03:35

Figure 5.3: Injection Results for O3 run

ing of the polarisation properties shown by gravitational waves.

Overall progress: The aforementioned enhancements serve to underscore the advancements achieved within the realm of gravitational wave astronomy. There has been notable progress in the retrieval of relevant data from a broader spectrum of celestial occurrences. Although a direct comparison between O3 events and O2 events is not feasible, these developments serve as evidence of the progress made in gravitational wave research and our capacity to derive significant insights from a growing range of astrophysical occurrences.

5.2.4 Statistics of chirp mass uncertainty

This analysis examines the variability of chirp mass values in gravitational wave occurrences and estimates the corresponding uncertainty. The estimation of the chirp mass is a pivotal task in comprehending the attributes of merged black holes.

The results given highlight the event-specific nature of chirp mass measurements and highlight the importance of rigorous investigation for each individual occurrence. Each event is depicted on the x-axis, with its unique chirp mass measurement and uncertainty. These numbers all fell within specified ranges. The chirp mass for event GW170104 in O2 was around 27.37, whereas event GW190425 in O3 had a chirp mass of approximately 28.09. Even though each occurrence revealed its own chirp mass value, this shows some sort of measuring consistency.

The uncertainty ranges for chirp mass measurements from O3 injections were somewhat less than those for O2 injections. This might indicate that our measures are becoming more accurate. In O2, for example, the chirp mass for event GW170809 had an uncertainty range of around 0.57 to 0.56, whereas in O3, the chirp mass for event GW190412 had an uncertainty range of about 0.53 to 0.52.

5.2.5 Statistics of mass ratio uncertainty for O2 & O3 injections

The error plots yielded many significant findings. The study examines the variations in mass ratios between O2 injections and O3 injections. Each event within

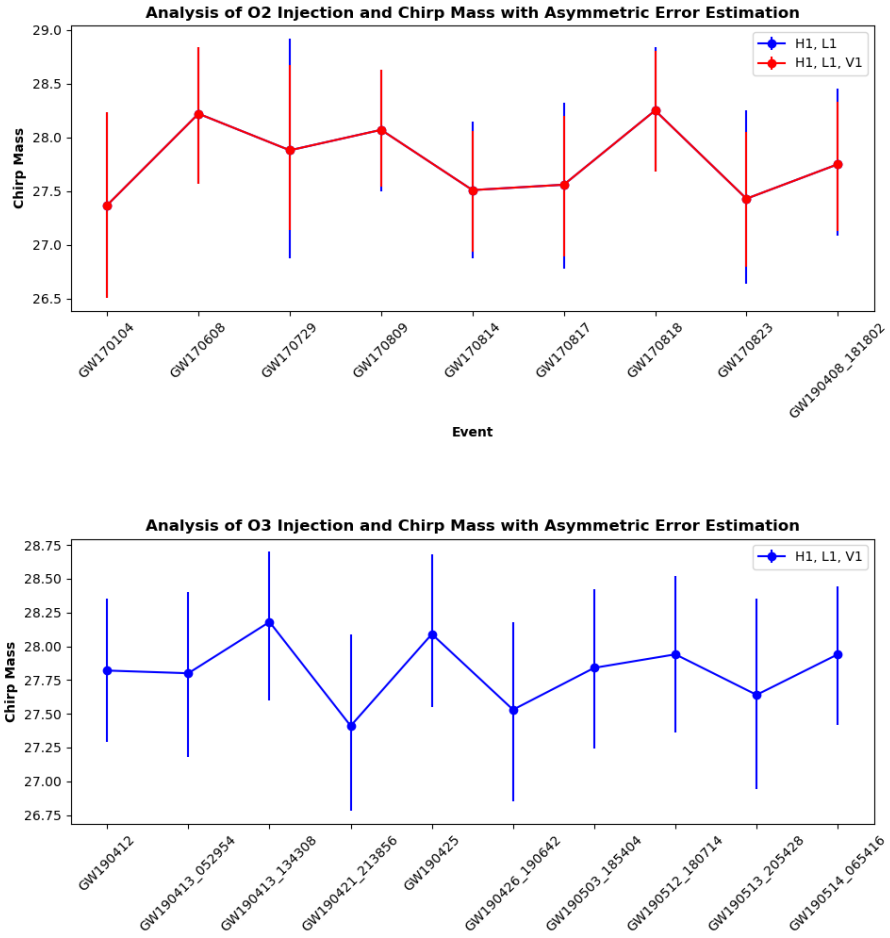

Figure 5.4: Chirp Mass Uncertainities and Detector Precision

the O2 and O3 injection sets exhibits distinct mass ratio values. It is worth noting that the mass ratio figures constantly fall within predetermined parameters. As an example, the mass ratio for event GW170104 in the second observing run (O2) was around 0.75, whereas event GW190425 in the third observing run (O3) exhibited a mass ratio of nearly 0.82.

The use of asymmetric error bars was carefully implemented to reflect the un-

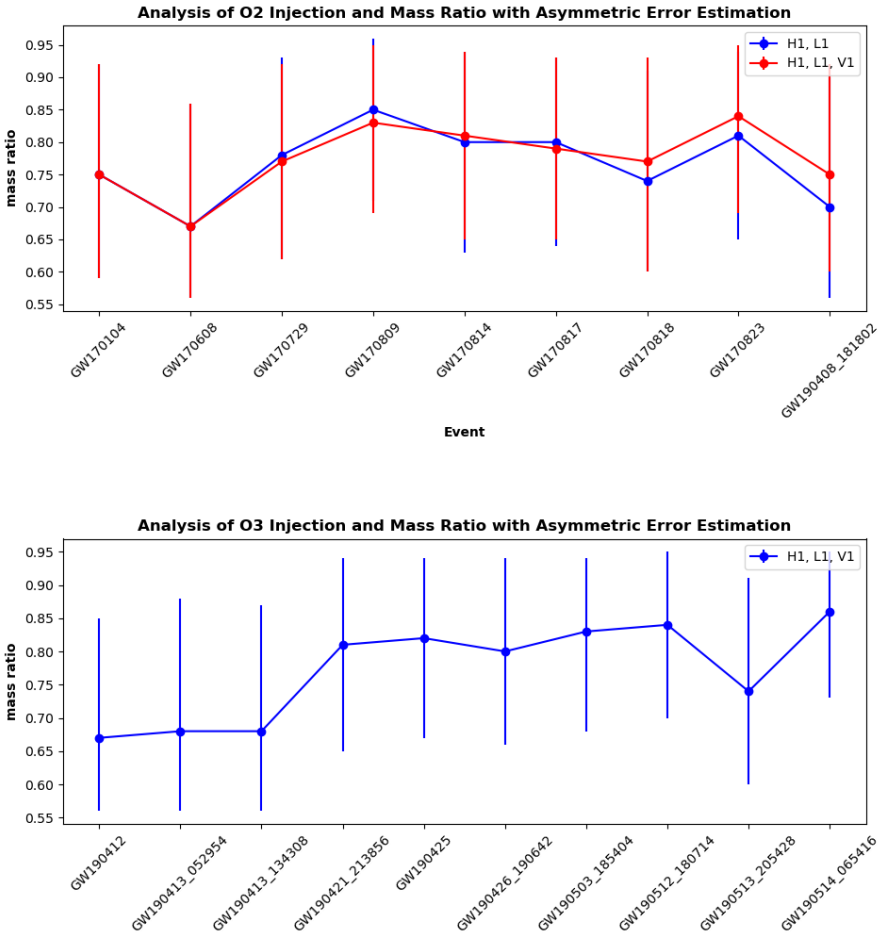

Figure 5.5: Mass Ratio Uncertainities and Detector Precision

certainty inherent in the measurements of mass ratios. The use of both upper and lower error bars in the study provides a thorough perspective on the uncertainties involved. In the case of O2, the lower error margin associated with GW170729 was roughly 0.16, while the higher error margin was around 0.15. This enhanced accuracy in measurement was crucial in refining the results.

The participation of the V1 detector in O3 injections has an observable effect

on mass ratio measurements. It is worth noting that O3 injections (H1, L1, and V1) have a lower range of error, indicating enhanced accuracy in measurement when compared to O2 injections (H1, L1).

Every event, which is shown on the x-axis, has its own distinct mass ratio value and corresponding uncertainty. The varied mass ratio values highlight the distinctiveness of the physical traits shown by each occurrence. As an example, the gravitational wave event GW170809 seen in the O2 data set had a mass ratio of around 0.85.

The analysis of O2 and O3 injections underscores the progressive improvement in measurement precision and the crucial significance of collaborative efforts among detectors. Significantly, the ranges of uncertainty for O3 injections (H1, L1, and V1) are getting narrower, which suggests that technology has made significant progress. As an example, the uncertainty interval for the gravitational wave event GW190514 during the third observing run (O3) was estimated to be roughly 0.09–0.17, highlighting the impact of the V1 detector.

The mass ratio is an essential quantity for understanding the dynamics of binary systems. The use of precise mass ratio measurements and the correct portrayal of errors significantly enhance the depth of analysis in the study of cosmic events. Within this particular context, the understanding of mass ratio is crucial, as event GW170814 with a mass ratio close to 0.80 demonstrates.

The data visualisations provided give a comprehensive view of the changes in mass ratios and the influence of detector participation. The arrangement of the content enables the examination of O2 and O3 injections, facilitating a deeper understanding of the progress made in the field of gravitational wave research.

5.2.6 Evaluating uncertainty in spin1 analysis

The results incorporate data obtained from three gravitational wave detectors, namely LIGO Hanford (H1), LIGO Livingston (L1), and Virgo (V1), enabling a comprehensive analysis including several detectors. The importance of asymmetric error estimates becomes apparent while striving to accurately characterise the mass ratio parameter, hence improving the dependability of gravitational wave parameter observations.

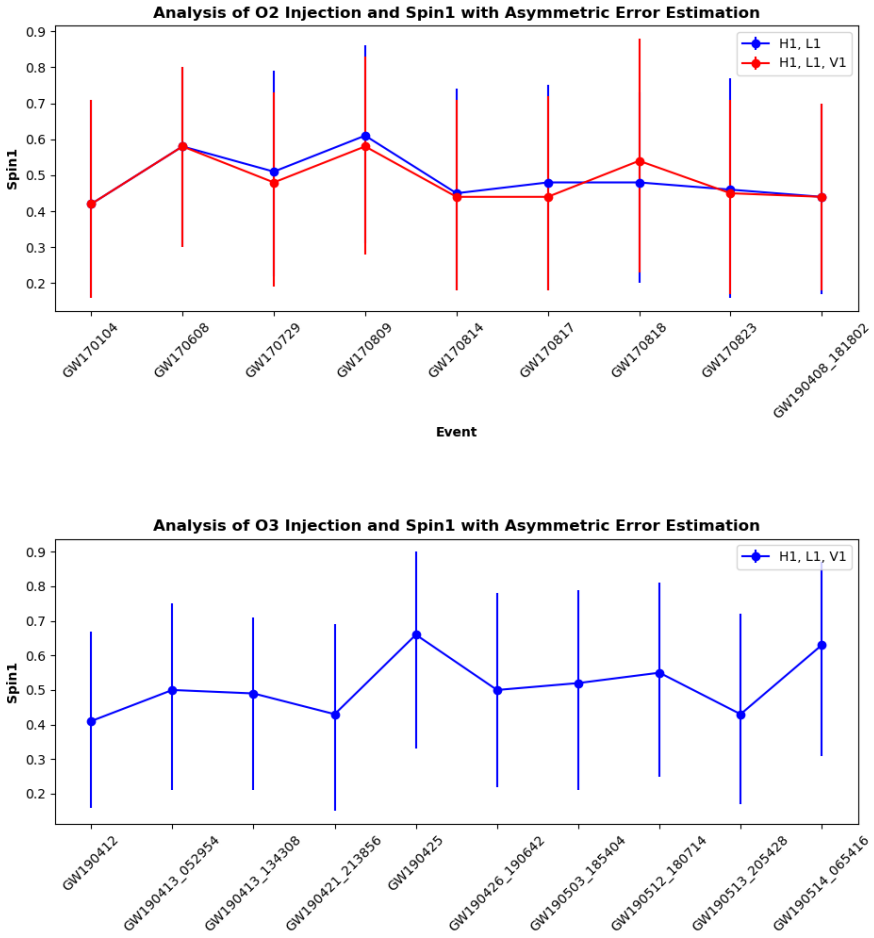

Figure 5.6: Spin1 Uncertainities and Detector Precision

The mass ratio is a metric of considerable significance since it characterises the relative masses of black holes that are undergoing mergers. The present study aims to examine the mass ratio parameter in a set of gravitational wave occurrences detected during the O2 and O3 observation sessions. We have chosen to examine incidents that were seen during both the O2 and O3 runs. The mass ratio parameter and its accompanying asymmetric errors have been documented

for each occurrence.

O2 observing run

The O2 Observing Run is a significant event in the field of astrophysics. The mass ratio parameters observed during the O2 observation run, namely for occurrences GW170104, GW170608, and GW170729, show a range of values. The use of asymmetric error estimation is vital, as it reveals lower errors ranges and higher errors ranges. The comparative analysis of data obtained from H1, L1, and V1 detectors highlights the valuable contribution of Virgo data in enhancing the accuracy of error estimates, with GW170814 serving as a particularly noteworthy example.

O3 observing run

The mass ratio parameter for the events seen during the O3 observation run, has a range between 0.67 and 0.86. Once again, we underscore the importance of using asymmetric error estimates. It is evident that the precise characterization of the mass ratio parameter necessitates the consideration of both lower and higher errors. The incorporation of data from the Virgo detector greatly enhances the accuracy of error estimates, notably in the case of the event GW190513_205428.

The significance of integrating data from numerous detectors and using asymmetric error estimation approaches is emphasised by our research, particularly in relation to the mass ratio parameter in gravitational wave occurrences. The incorporation of Virgo detector data in both the O2 and O3 runs significantly contributes to the improvement of accuracy and reliability in mass ratio determinations.

Our study has significantly enhanced our comprehension of the mass ratio parameter in gravitational wave phenomena. The aforementioned statement highlights the importance of asymmetric error estimates and the incorporation of data from different detectors.

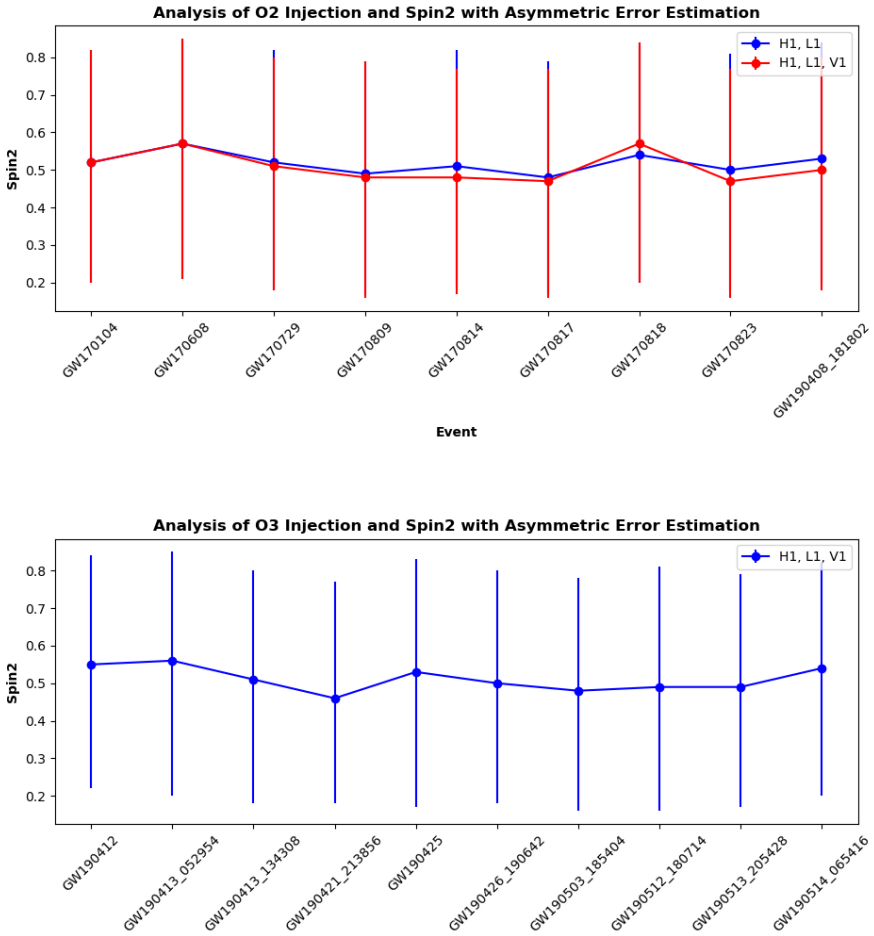

Figure 5.7: Spin2 Uncertainities and Detector Precision

5.2.7 Quantifying uncertainty in spin2 analysis

The error plots for Spin2 yielded many significant findings. The study examines the variability in O2 injections (H1, L1) and O3 injections (H1, L1, V1) in Spin2. In both the O2 and O3 injection scenarios, there are big differences in how Spin2 is measured when gravitational waves happen in different ways. Every event demonstrates a specific Spin2 value, which signifies the unique attributes of these

astrophysical occurrences. As an example, the event GW170608 in the O2 dataset had a Spin2 value of roughly 0.57.

Enhancing accuracy through asymmetrical error estimation: The use of asymmetric error bars serves as a viable method for incorporating uncertainty related to Spin2 readings. The use of higher and lower error bars in this complete methodology significantly improves the accuracy of Spin2 readings. In the O2 dataset, it was observed that the lower error associated with the GW170814 event was roughly 0.31, while the higher error was found to be approximately 0.31 as well.

The impact of collaborative efforts on the study of spin2: The incorporation of the V1 detector in O3 injections has a discernible influence on Spin2 readings. The O3 injections (H1, L1, V1) exhibit fluctuations in Spin2 with uncertainty ranges that are considerably smaller in comparison to the O2 injections (H1, L1). This suggests an improvement in the accuracy of the measurements. As an example, the event GW190421_213856 seen in O3 demonstrated a narrower range of uncertainty, characterised by a lower limit of roughly 0.28 and an upper limit of 0.31.

Analysis of spin2 in relation to a specific event: Every event, which is shown on the x-axis, has its own unique Spin2 value and corresponding uncertainty. The wide range of Spin2 values observed highlights the distinct properties shown by each gravitational wave occurrence. As an example, the event GW170729 in the O2 dataset had a Spin2 value almost equal to 0.52.

A comparative analysis of mass ratio and spin in a theoretical framework: While Spin2 displays distinct changes, a comparison study with Mass Ratio and Spin1 shows contrasting patterns and behaviours within these astrophysical phenomena. The integration of these studies offers a thorough comprehension of the properties and behaviours of gravitational wave occurrences across many parameters, making a valuable contribution to the wider domain of astrophysics study. By delineating the disparities between the outcomes pertaining to Spin2 and those concerning Mass Ratio and Spin1, we accentuate the distinct characteristics and fluctuations linked to each parameter, facilitating a more intricate comprehension of the gravitational wave phenomena now under scrutiny.

5.3 Designed HLV

The results presented in this study stem from an analysis 4.4 titled "Simulating and analysing gravitational wave signals in a future network of detectors". These results offer a detailed description of the approach employed to incorporate gravitational wave data into an established network of detectors.

In the results, specific parameter values for gravitational wave injection are used. Notable values encompass a_1 at 0.40, a_2 at 0.30, θ_1 at 0.50, θ_2 at 1.00, ϕ_{12} at 1.70, ϕ_{jl} at 0.30, luminosity_distance at 2000, ψ at 2.659, and "phase" at 1.30. These values play pivotal roles in determining the behaviour and characteristics of the GWs under study, exerting influence over the outcomes of the research.

It is noteworthy to mention that the aforementioned signal injections are intended for future implementation, with temporal reference made to the Earth's centre, and they span a variety of frequency ranges.

The main objective of this investigation is to explain the estimated parameters associated with the injected gravitational wave signals. Two separate iterations, "run1" and "run2," each adhering to predetermined setups and limits, accomplish this. The primary aim is to gain significant knowledge about the fundamental attributes of these gravitational wave signals.

The subsequent findings pertain to the changes and modifications carried out in this study. The study comprises two distinct phases, denoted run 1 and run 2, which involve a modification in the minimum frequency threshold employed for detecting gravitational wave signals. During the initial round, signals with frequencies of 10 Hz and above are considered, while in the subsequent round, this threshold is heightened to frequencies of 20 Hz and above.

The mass ratio and chirp mass undergo changes from their original input values, which is worth noting. In the study labelled "run1," the mass ratio tends to approach a value of $0.84^{+0.11}_{-0.15}$, while the chirp mass undergoes a transition to $28.19^{+0.11}_{-0.12}$. In the study titled "run2," it have improved the estimation of the mass ratio, which is now reported as $0.85^{+0.11}_{-0.15}$. Additionally, the chirp mass has

Table 5.2: Parameter Settings for Gravitational Wave Injection

Parameters	**Input**	**Injection**	**Injection**
Run		run1	run2
Detectors		H, L1, V1	H1, L1, V1
geocent_time	1502019943		
nlive		512	512
walks		100	100
n_check_point		5000	5000
dlogz		0.2	0.2
psd_frequency		>= 10	>= 20
q	0.8	$0.84^{+0.11}_{-0.15}$	$0.85^{+0.11}_{-0.15}$
chirpmass	28.09	$28.19^{+0.11}_{-0.12}$	$28.21^{+0.11}_{-0.12}$
mass_1	36	35.36	35.17
mass_2	29	29.70	29.90
theta_jn	0.40	$0.75^{+0.39}_{-0.35}$	$0.75^{+0.36}_{-0.37}$
dec	-1.21	$1.20^{+0.03}_{-0.03}$	$1.20^{+0.03}_{-0.03}$
ra	1.375	$1.37^{+0.02}_{-0.02}$	$1.37^{+0.02}_{-0.02}$
duration (hrs)		10.59	7.13

been determined to be $28.21^{+0.11}_{-0.12}$. These transitions serve as examples of enhanced precision in parameter estimates.

The study results in modifications to the masses of the components (mass_1 and mass_2) inside the binary black hole system. In the run 1 experiment, the masses undergo a change to 35.36 and 35.17 respectively. Similarly, in the "run2" experiment, the masses are modified to 29.70 and 29.90. These transitions highlight the level of accuracy attained in calculating these crucial factors.

The refinement of the inclination angle (θ_{jn}) involves a transition from its starting value of 0.40. The estimated value in "run1" is around $0.75^{+0.39}_{-0.35}$, whereas in "run2" it is further refined to $0.75^{+0.36}_{-0.37}$. This transition denotes improved precision in characterising the alignment of the binary black hole system.

The study comprises the estimation of declination (dec) and right ascension (ra) angles. The angles for both "run1" and "run2" exhibit a transition to values of $1.20^{+0.03}_{-0.03}$ and $1.37^{+0.02}_{-0.02}$, respectively. This observation highlights the accurate localisation of the gravitational wave source.

Length variation: The analysis runs exhibit variation in length, with run 1 having a duration of 10.59 hours and run 2 having a duration of 7.13 hours. This variance takes into consideration the disparities in the duration of data collection.

The aforementioned important results highlight the modifications and enhancements implemented throughout the research process, leading to enhanced parameter estimations for gravitational wave signals. Additionally, they emphasise the effectiveness of the analytic approach in accurately characterising signals of this kind.

The data shown in corner plot5.8 for parameter "psd_frequency": >= 10 for "Injection run1" and corner plot for >= 20 for "Injection run2" doesn't have much difference. Since, the aforementioned numbers denote the minimum threshold of the frequency spectrum used in the study of GWs. The lack of discernible distinction between these two quantities may be attributed to the inherent properties of gravitational wave transmissions and the level of sensitivity shown by the detectors. GWs emanating from astronomical sources often exhibit frequencies that beyond the 10 Hz threshold, frequently spanning from tens to hundreds of Hz or even exceeding these values. Hence, the choice between setting the lower limit at 10 Hz or 20 Hz does not provide a significant disparity, since both thresholds include the relevant frequency spectrum for gravitational waves, which mostly manifest at far higher frequencies.

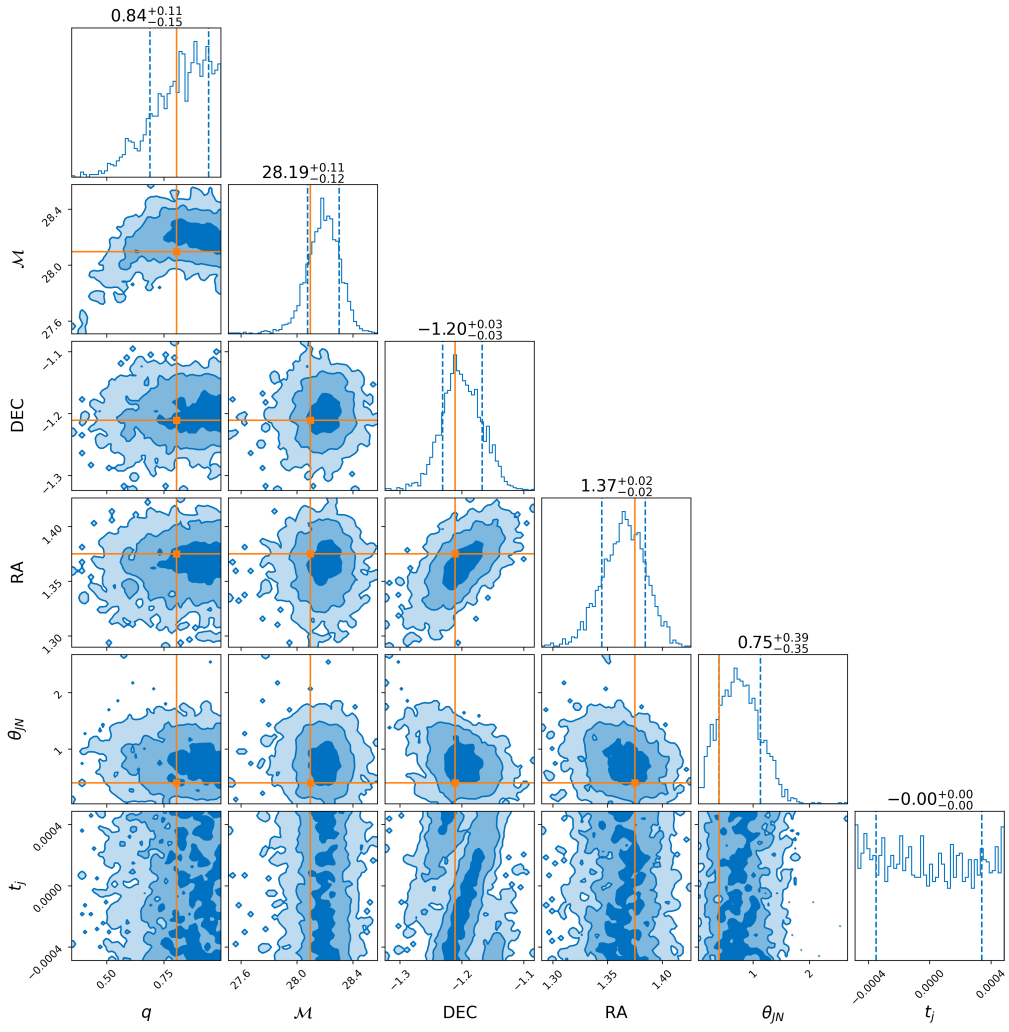

Figure 5.8: corner plot for 10 Hz with designed HLV

Chapter 6

Conclusions

In conclusion, this work, facilitated by the code used throughout the study, has delved into the estimation of the source properties of GWs resulting from black hole collisions, a significant area of research in modern astrophysics. Through the meticulous application of statistical techniques, Bayesian inference, and advanced sampling methods, a deeper understanding of the source parameters characterising gravitational wave signals has been achieved.

The analysis, which included a full look at GW150914 under different parameter settings and insights into the properties of the injected GWs across different observational runs, has given the field important new information. Furthermore, statistical assessments of mass ratios and spin uncertainties have shed light on the intricacies of these phenomena.

Moreover, the code employed in this research holds the potential for broader applications, particularly in simulating scenarios for future detectors. As demonstrated by simulating future PSDs, it opens up avenues to anticipate and prepare for the challenges and opportunities that lie ahead in the study of GWs.

Looking ahead, this work opens avenues for future research. Expanding detector networks, refining estimation techniques, and exploring additional sources of GWs are promising directions to deepen cosmic insights. In particular, the introduction of the concept of a future detector network, HLV, underscores the potential for enhanced gravitational wave analysis.

To understand future observations better, continued efforts should focus on refining modeling, improving the sensitivity and accuracy of detectors, and developing advanced data analysis techniques, all of which can be informed by the code used for simulating future scenarios. Addressing these challenges will enable further exploration of GWs and their origins, ultimately unravelling more of the universe's mysteries.

Bibliography

[1] A. A. Coley and D. L. Wiltshire, "What is general relativity?" *Physica Scripta*, vol. 92, no. 5, p. 053001, 2017.

[2] B. C. Barish and R. Weiss, "Ligo and the detection of gravitational waves," *Physics Today*, vol. 52, no. 10, pp. 44–50, 1999.

[3] Q. Yu, "Evolution of massive binary black holes," *Monthly Notices of the Royal Astronomical Society*, vol. 331, no. 4, pp. 935–958, 2002.

[4] G. Baym and C. Pethick, "Neutron stars," *Annual Review of Nuclear Science*, vol. 25, no. 1, pp. 27–77, 1975.

[5] D. H. Clark and F. R. Stephenson, *The historical supernovae*. Elsevier, 2016.

[6] U. of Birmingham. Gravitational waves explained. [Online]. Available: https://www.birmingham.ac.uk/research/gravitational-wave/gravitational-waves-explained.aspx

[7] J. H. Taylor Jr, "Binary pulsars and relativistic gravity," *Reviews of Modern Physics*, vol. 66, no. 3, p. 711, 1994.

[8] V. Frolov and I. Novikov, *Black hole physics: Basic concepts and new developments*. Springer Science & Business Media, 2012, vol. 96.

[9] T. Chiba and T. Nakamura, "The luminosity distance, the equation of state, and the geometry of the universe," *Progress of theoretical physics*, vol. 100, no. 5, pp. 1077–1082, 1998.

[10] A. Lyne, "Orbital inclination and mass of the binary pulsar psr0655+ 64," *Nature*, vol. 310, no. 5975, pp. 300–302, 1984.

[11] A. Abramovici, W. E. Althouse, R. W. Drever, Y. Gürsel, S. Kawamura, F. J. Raab, D. Shoemaker, L. Sievers, R. E. Spero, K. S. Thorne *et al.*, "Ligo: The laser interferometer gravitational-wave observatory," *science*, vol. 256, no. 5055, pp. 325–333, 1992.

[12] R. Weiss, "Nobel lecture: Ligo and the discovery of gravitational waves i," *Reviews of Modern Physics*, vol. 90, no. 4, p. 040501, 2018.

[13] C. Cutler and K. S. Thorne, "An overview of gravitational-wave sources," *General Relativity and Gravitation*, pp. 72–111, 2002.

[14] J. Joyce, "Bayes' theorem," 2003.

[15] D. Van Ravenzwaaij, P. Cassey, and S. D. Brown, "A simple introduction to markov chain monte–carlo sampling," *Psychonomic bulletin & review*, vol. 25, no. 1, pp. 143–154, 2018.

[16] E. W. Weisstein, "Normal distribution," *https://mathworld. wolfram. com/*, 2002.

[17] L. S. Collaboration. Dynesty guide. [Online]. Available: https://lscsoft.docs.ligo.org/bilby/dynesty-guide.html

[18] Wikipedia. Chirp mass. [Online]. Available: https://en.wikipedia.org/wiki/Chirp-mass

[19] C. Cutler and E. E. Flanagan, "Gravitational waves from merging compact binaries: How accurately can one extract the binary's parameters from the inspiral waveform?" *Physical Review D*, vol. 49, no. 6, p. 2658, 1994.

[20] G. P. Sutton and O. Biblarz, *Rocket Propulsion Elements, 7th Edition*. John Wiley & Sons, 1992.

[21] L. S. Collaboration. Bilby api documentation: lal_binary_black_hole. [Online]. Available: https://lscsoft.docs.ligo.org/bilby/api/bilby.gw.source.lal_binary_black_hole.html